ASME Paper Title: CFD investigation of a core-mounted-target-type thrust reverser,

Part 2: reverser deployed configuration

Authors: Mahmood T, Jackson AJB, Sethi V, Khanal B, Ali F

ASME Journal Title: Journal of Engineering for Gas Turbines and Power

Volume/Issue __140, Issue 9_____ Date of Publication (VOR* Online) _25 December 2017_

ASME Digital Collection URL: http://gasturbinespower.asmedigitalcollection.asme.org/article.aspx?articleid=2667892

DOI: 10.1115/1.4038817

Journal of Engineering for Gas Turbines and Power
Volume 140, Issue 9, September 2018, 091205
Paper number: GTP-17-1465

CFD Investigation of a Core-Mounted-Target-Type Thrust Reverser, Part 2: Reverser Deployed Configuration

Tashfeen Mahmood[1]

Email: dr.tashfeenmahmood@gmail.com
Defence Equipment and Services, Ministry of Defence,
Bristol, BS34 8JH, UK

Anthony Jackson[2]

Email: a.j.b.jackson@cranfield.ac.uk
Cranfield University, Centre for Propulsion Engineering,
Bedfordshire, MK43 0AL, UK

Vishal Sethi[3]

Email: v.sethi@cranfield.ac.uk
Cranfield University, Centre for Propulsion Engineering,
Bedfordshire, MK43 0AL, UK

Bidur Khanal[4]

Email: b.khanal@cranfield.ac.uk
Cranfield University, Centre for Defence Engineering,
Shrivenham, SN6 8LA, UK

Fakhre Ali[5]

Email: fakhre.ali@chalmers.se
Chalmers University of Technology, Applied Mechanics Department,
Hörsalsvägen 7A, Göteborg, Sweden

[1] Engineering Manager
[2] Senior Research Companion
[3] Lecturer
[4] Lecturer
[5] Research Fellow

Abstract

Core Mounted Target Type Thrust Reverser (CMTTTR) design was proposed by NASA in the second half of the 90's. NASA carried out several experiments at static conditions, and their acquired results suggested that the performance characteristics of the CMTTTR design falls short to comply with the mandatory TR performance criteria, and were therefore regarded as an infeasible design. However, the authors of this paper believe that the results presented by NASA for CMTTTR design require further exploration to facilitate the complete understanding of its true performance potential. This Part 2 paper is a continuation from Part 1 (reverser stowed configuration) and presents a comprehensive three-dimensional Computational Fluid Dynamics (CFD) analyses of the CMTTTR in deployed configuration. The acquired results are extensively analysed for aforementioned configuration operating under the Static Operating Conditions at Sea Level i.e. SLS, ISA; the analyses at forward flight conditions will be covered in Part 3. The key objectives of this paper are: first, to validate the acquired CFD results with the experimental data provided by NASA: this is achieved by measuring the static pressure values on various surfaces of the deployed CMTTTR model. The second objective is to estimate the performance characteristics of the CMTTTR design and corroborate the results with experimental data. The third objective is to estimate the Pressure Thrust (i.e. axial thrust generated due to the pressure difference across various reverser surfaces) and discuss its significance for formulating the performance of any thrust reverser design. The fourth objective is to investigate the influence of kicker plate installation on overall TR performance. The fifth and final objective is to examine and discuss the overall flow physics associated with the thrust reverser under deployed configuration.

Nomenclature

3D	=	Three Dimensional
AMTTR	=	Annular (Metal) Type Thrust Reverser
A_{fan}	=	Fan nozzle physical exit area
A_{rev}	=	Reverser physical exit Area
BPR	=	Bypass Ratio
CAD	=	Computer Aided Design
CFD	=	Computational Fluid Dynamics
CMTTTR	=	Core Mounted Target Type Thrust Reverser
CTTR	=	Cascade Type Thrust Reverser
CUTS_TF	=	Cranfield University Twin Spool Turbofan
D_{rev}	=	Reverser diameter
FNPR	=	Fan nozzle pressure ratio
FOD	=	Foreign Object Damage
F_A	=	Axial Thrust [kN]
F_{Core}	=	Core Thrust [kN]
$F_{Core\ Thrust,\ Rev\ Deployed}$	=	Core Thrust during reverser deployment [kN]
F_{Fan}	=	Fan Gross Thrust [kN]
$F_{Pressure\ Thrust}$	=	Pressure Thrust [kN]
$F_{Resultant\ Thrust,\ T/Rev\ Deployed}$	=	Resultant Thrust [kN], $\sqrt{F_X{}^2 + F_Y{}^2 + F_Z{}^2}$
$F_{Total\ Fwd.\ Thrust}$	=	Total Forward Thrust (i.e. Fan + Core) [kN]
$F_{Total,\ Decelerating\ Thrust}$	=	Total Decelerating Thrust [kN], $F_{Momentum\ Drag} + F_{Pressure\ Thrust} + F_X - F_{Core,\ T/Rev\ Deployed}$
F_X	=	Reverser Thrust Axial Component [kN]
F_Y	=	Reverser Thrust Radial (i.e. vertical) Component [kN]
F_Z	=	Reverser Thrust Side Force Component [kN]
HBPR	=	High bypass ratio
NASA	=	National Aeronautics and Space Administration
NPR	=	Nozzle Pressure Ratio

RAR	=	Reverser Area Ratio, (A_{rev} / A_{fan})
SLS	=	Sea Level Static (i.e. M=0 at ISA conditions)
TR	=	Thrust Reverser
$\dot{W}_{Rev,\ Thrust}$ / $\dot{W}_{Fwd,\ Thrust}$	=	Mass flow ratio
ℓ	=	Horizontal distance between the fan nozzle and the CMTTTR
η_{Fan}	=	Fan Reverser Effectiveness
η_{Rev}	=	Overall Reverser Effectiveness
$\eta_{Rev,2}$	=	Overall Reverser Effectiveness with Pressure Thrust

1. Introduction

The trend of higher Bypass Ratios (BPRs) on civil turbofan engines is likely to continue, and it seems plausible that the future turbofan engines will have BPR values as high as 15 [1]. This implies that the future high BPR engines will employ a larger fan, hence a much larger diameter bypass nacelle, and as a result are likely to be heavier and wider than existing turbofans. The weight and size of the future high BPR engines will also impose additional constraints on thrust reversers, landing gear lengths and runway clearance. For the TR designer, such high BPR engines will introduce unique challenges, primarily due to the fact that the future reverser designs will be larger, heavier, and will require more robust actuation and control systems.

Thrust reversers on high BPR engines (i.e. BPR>6) are limited to Cascade Type Thrust Reverser (CTTR) design, and although the TRs on modern aircraft such as A380 and B787 have adopted advanced lightweight materials along with use of electrical control systems, the fundamental design of the CTTR hasn't changed significantly since the 1960s, and it is likely to be the only feasible design candidate for future high BPR engines. Therefore, it is imperative that the aerospace community must proactively conduct research to explore and develop innovative and breakthrough TR designs. Any new TR design must offer weight savings and possible improvements in reverser efficiency and performance. Other secondary areas to consider are: sealing, locking mechanisms, actuation and control systems, maintainability and ease of access for repair and overhauls. These parameters will benefit airline economics, reduce fuel consumption, improve brake life and offer greater safety of aircraft and passengers.

In the mid-90s, NASA investigated six novel thrust reverser designs and Annular Metal Target Thrust Reverser (AMTTR) is one of them [1]; in this paper, AMTTR is referred as the Core Mounted Target Type Thrust Reverser

(CMTTTR). The CMTTTR design utilizes existing surfaces of the core nacelle outer cowl and uses them to re-direct the bypass flow (i.e. act as a TR), (Fig 1). This is an innovative approach to TR design; it eliminates the complete TR assembly from the bypass nacelle, which means there will be no need to have cascade blocks, blocker doors and translating cowl. The nacelle design engineer can thus use this opportunity to further optimize the fan nacelle shape, structure and size.

In the experiments carried out by NASA, eight different CMTTTR configurations were investigated, however, the results were not very promising [1]; it was observed that all the CMTTTR configurations failed to meet the standard reverser effectiveness criteria of 40% by a considerable margin. Literature review failed to find any significant work on the CMTTTR concept. However, the authors of this paper believe that it is sensible to further investigate the CMTTTR design using 3D CFD analyses; CFD study can provide an insight into the deficiencies of the CMTTTR design and perhaps could be a stepping stone for future work.

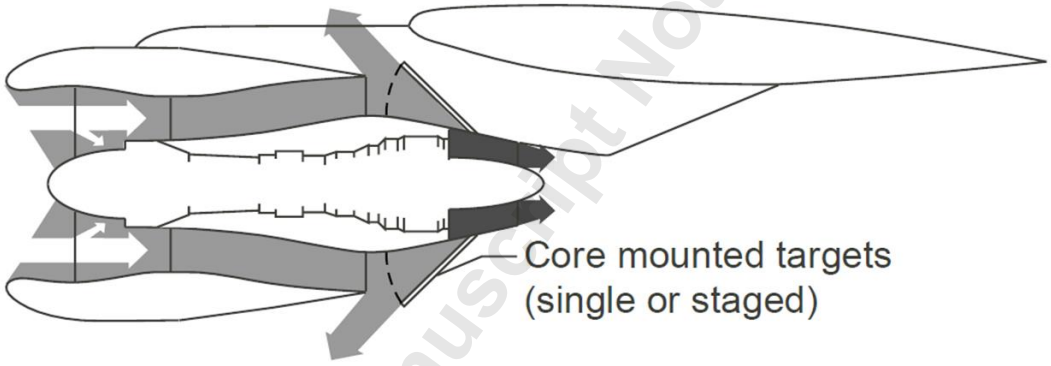

Fig. 1: Conceptual layout of an Annular Metal Target Type Thrust Reverser, also referred in this paper as CMTTTR, adopted from [1].

2. Employed Simulation Methodology

The simulation methodology employed here is similar to Part 1 [2], thus, only those areas which are specifically relevant to the current CMTTTR deployed configuration are addressed. The overall methodology is accomplished using the following four broad steps:

(i) 3D CAD model is compiled using the following parts: engine, pylon, wing, CMTTTR, kicker plate, runway, symmetry and far field boundaries.

(ii) Mesh is generated on the assimilated 3D CAD model to support the CFD analyses.

(iii) Setting up the CFD cases, i.e. selection of fluid properties, discussion on solver, turbulence models, convergence criteria etc.

(iv) Engine performance study to obtain reasonable boundary conditions for all of the CFD cases.

2.1 Compilation of 3D CAD models and computational setup

The static tests on the CMTTTR were performed by NASA on a 7.9% scale model of a GE-90 engine (Fig 2 and 3); however, for the implementation of the CFD study, full-scale 3D CAD models are developed for the CMTTTR deployed configuration, as shown in Fig. 4-6.

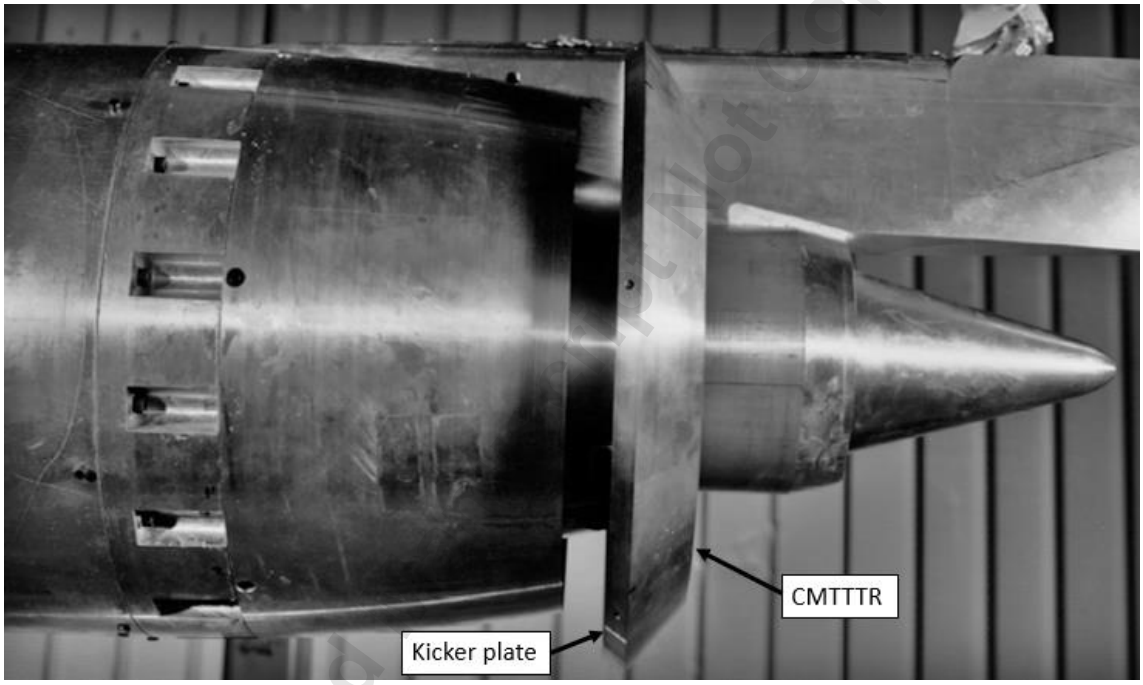

Fig. 2: Wind tunnel model of the TR in deployed configuration, adopted from [1].

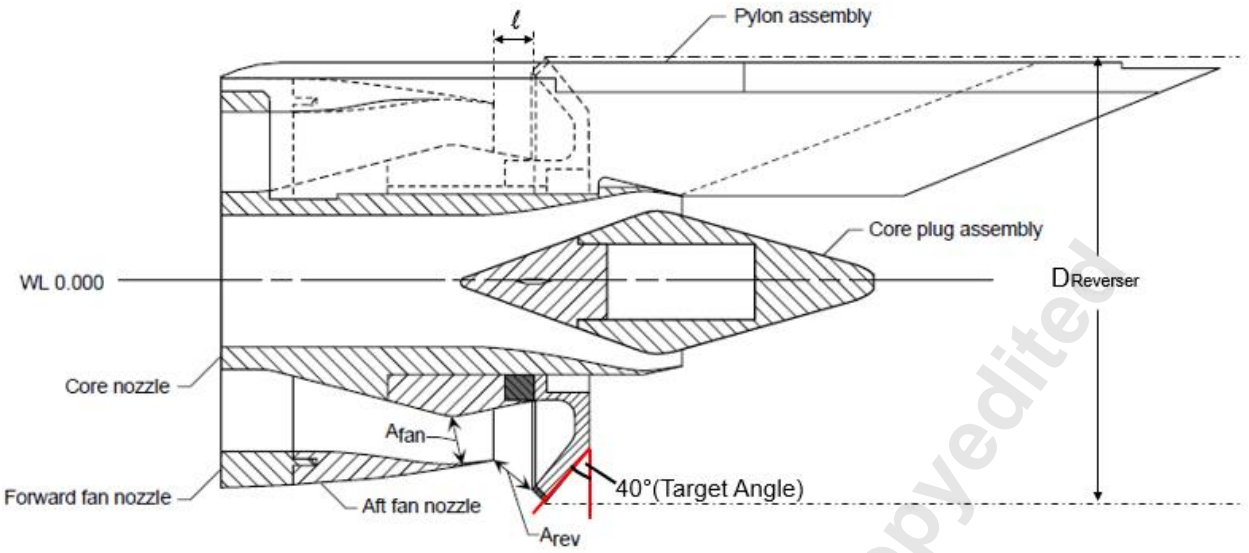

Fig. 3: Cross-sectional view of the CMTTTR, adopted from [1].

All experiments were conducted in the Jet Exit Test Facility at NASA Langley Research Centre [1]. In total eight different CMTTTR configurations were investigated; the three primary design parameters in the experiments were the reverser area ratio (RAR), target angle, and installation of a kicker plate. The summary of all the CMTTTR configurations is presented in [Table 1]. For the 3D CFD study, configurations 7 and 8 are selected; these configurations in the test report [1] are referred as configuration 307 and 308, the Test number was 987 and the Test Runs were Run 35 and 36 [1]. The only difference between the two configurations is the installation of kicker plate as tabulated in Table 1.

Table 1: Difference between Experimental and Computational Setup

No	Tests	Target Angle	Kicker Plate	FNPR	Flow Through	Wing Installed	Rev Area Ratio	Runway
1	Experiment	20 degree	No	1.0<NPR≤2.0	Supply lines	No	1.05	No
2	Experiment	20 degree	No	1.0<NPR≤2.0	Supply lines	No	1.15	No
3	Experiment	20 degree	No	1.0<NPR≤2.0	Supply lines	No	1.25	No
4	Experiment	20 degree	Yes	1.0<NPR≤2.0	Supply lines	No	1.25	No
5	Experiment	40 degree	No	1.0<NPR≤2.0	Supply lines	No	1.05	No
6	Experiment	40 degree	No	1.0<NPR≤2.0	Supply lines	No	1.15	No

7	Experiment	40 degree	No	1.0<NPR≤2.0	Supply lines	No	1.25	No
8	Experiment	40 degree	Yes	1.0<NPR≤2.0	Supply lines	No	1.25	No
7A	CFD	40 degree	No	1.0<NPR≤1.65	Nacelle	Yes	1.25	Yes
8B	CFD	40 degree	Yes	1.0<NPR≤1.65	Nacelle	Yes	1.25	Yes

In the experiments, primary and secondary flows were drawn using the supply lines; the supply lines were connected to the external source. The use of supply lines is not a feasible approach to support execution of CFD analyses, therefore complete nacelle models are developed and implemented, as shown in Fig. 4. Table 1 summarizes the differences between the designs employed during the experiments and those employed within this study to implement the CFD analyses.

All the CMTTTR experiments were performed without a wing and runway surfaces; however, the objective of the CFD study is to represent a realistic scenario and for this purpose, both the wing and the runway models are included as depicted in Fig. 5 and [Table 1]. The inclusion of a runway is important for the CFD analyses; it will allow understanding of the complex flow physics associated between the reverser exhaust plumes and the ground. The impingement of reverser exhaust flow on the ground will provide an insight into the areas of interest such as FOD (Foreign Object Damage), flow ingestion, temperature and pressure distortions etc. To fully capture the reverser flow behavior underneath the nacelle, the runway is divided into two sections as shown in Fig. 5 and 6. The runway surface within the immediate vicinity of the nacelle benefits from a refined mesh, which will aid the flow visualization and will facilitate an in-depth understanding of complex flow physics associated with the region.

Another important requirement for successful execution of the CFD analyses is to have a sufficiently large flow domain. The pressure far fields in the upstream and downstream zones are set as ≈60 times the size of the wingspan: the height of the flow domain is ≈30 times the size of wing span, Fig. 5; the interested reader can refer to Part 1 for more details.

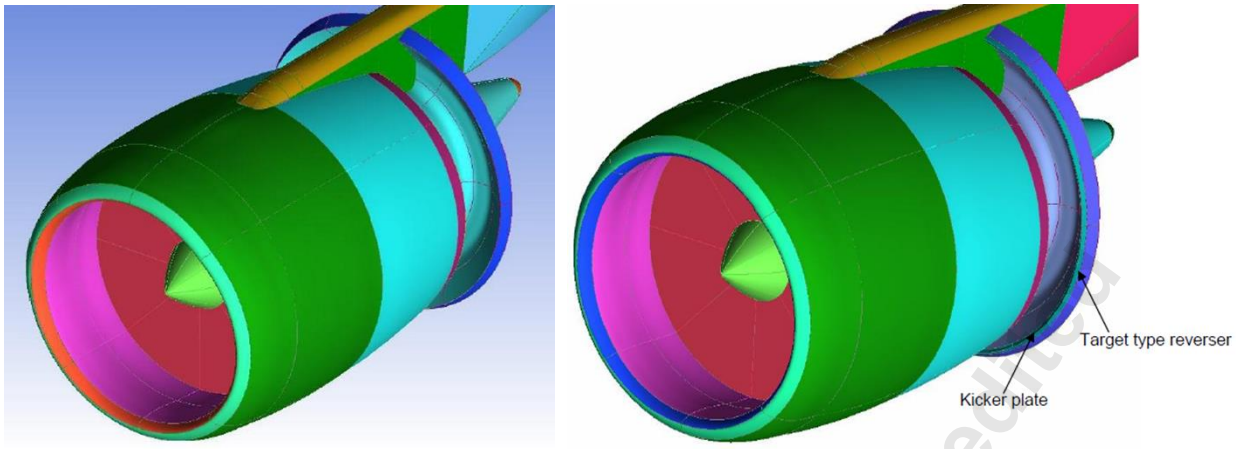

Fig. 4: 3D CAD models of a HBPR≈9 engine, employing a CMTTTR with and without kicker plate.

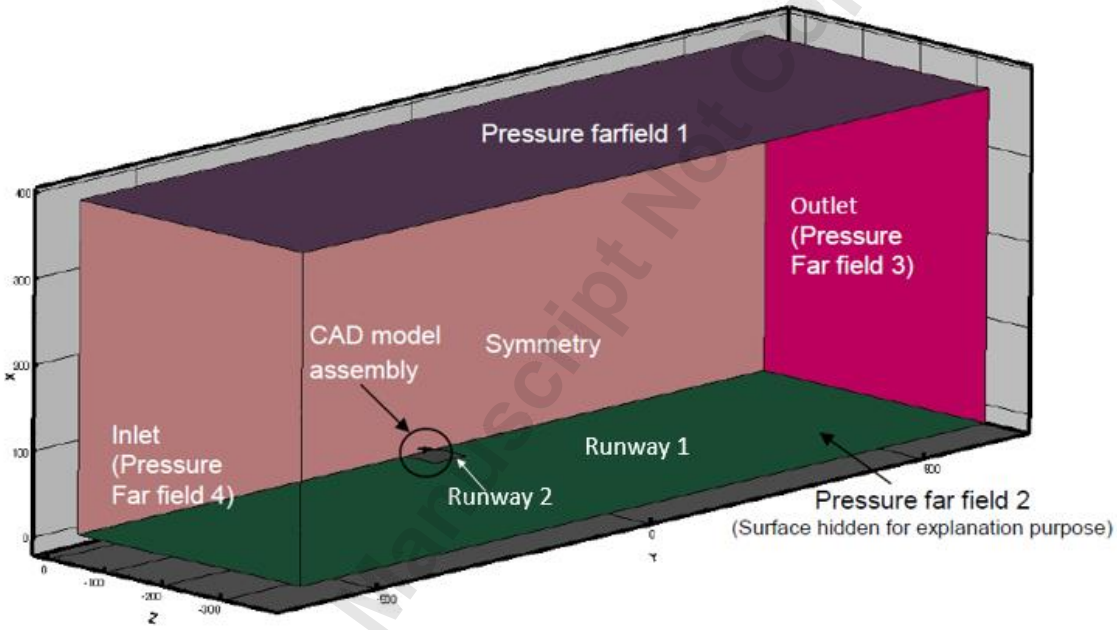

Fig. 5: An isometric view of the complete 3D CAD model used for this CFD study.

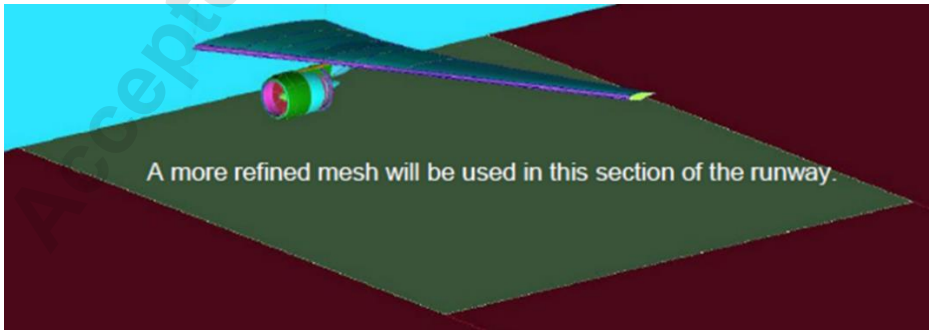

Fig. 6: Two runway surfaces are built. The surface immediately under the nacelle will have a refined mesh; this will help understanding the complex flow physics underneath the nacelle.

One of the key performance requirements for any TR design is to satisfy the engine mass flow compatibility criteria. This can be explained by assuming, that the TR is deployed, and the engine is throttled to 80% thrust power: at this thrust setting the mass flow through the TR should approximately be equal to that expected in the forward thrust configuration. This, with the appropriate reverser effective nozzle area, is an essential performance criterion and will ensure that the operating points on the compressor maps are not affected by the TR deployment (i.e. the engine off-design performance, during reverser deployment must approximately be similar to that of the forward thrust configuration). Also, TR deployment must have a minimal effect on the performance of other engine components. However, achieving this mass flow compatibility during TR deployment is difficult; this is mainly because the bypass flow through the fan nozzle is generally axial, whereas, in the reverse thrust configuration, the flow is first forced to turn at an angle due to the presence of the blocker door and later is guided using the TR target surface, as shown in (Fig. 7). A common approach to fulfilling this mass flow compatibility criteria for the reverser deployed configurations is to iteratively find an '*effective reverser exit area'* which will satisfy this condition. Generally, the '*effective reverser exit area'* is set slightly larger than the '*forward nozzle effective area'* to ensure that the engine will maintain sufficient surge margin. This is particularly important during engine transient operations; a typical example is when an aircraft lands, the pilot selects the reverse thrust lever and changes the engine settings from forward idle to reverse idle, and from reverse idle to maximum reverse (i.e. 80% power) in approximately 3 seconds.

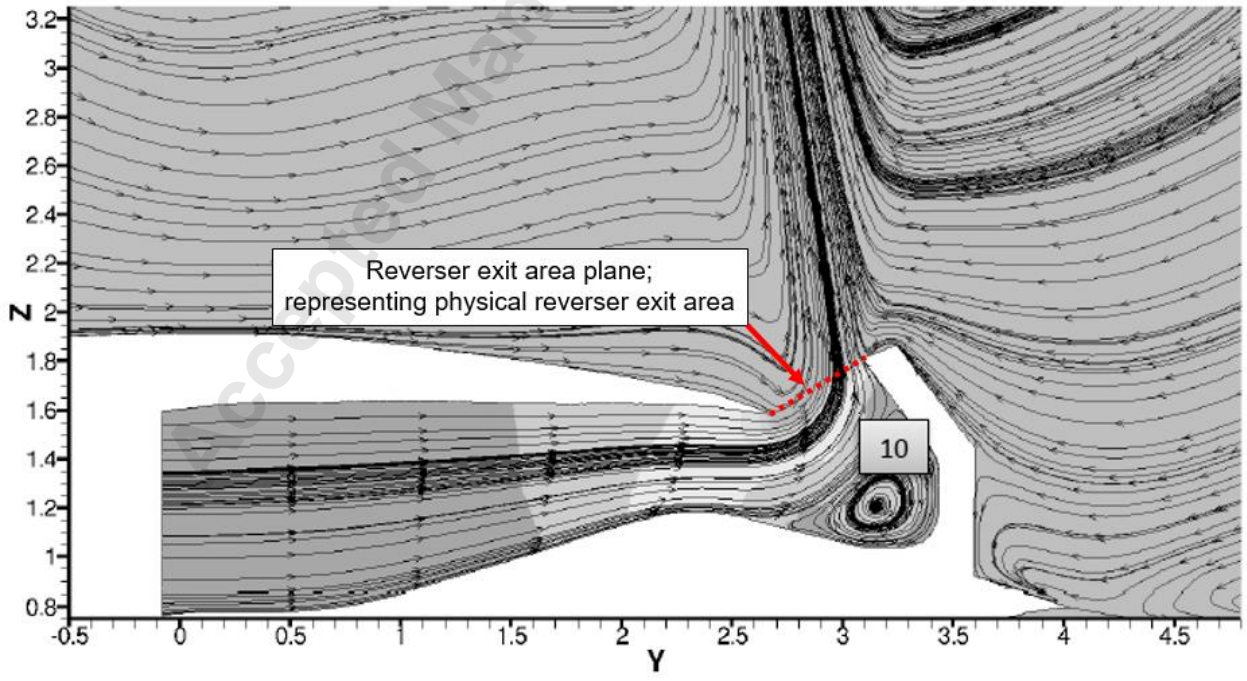

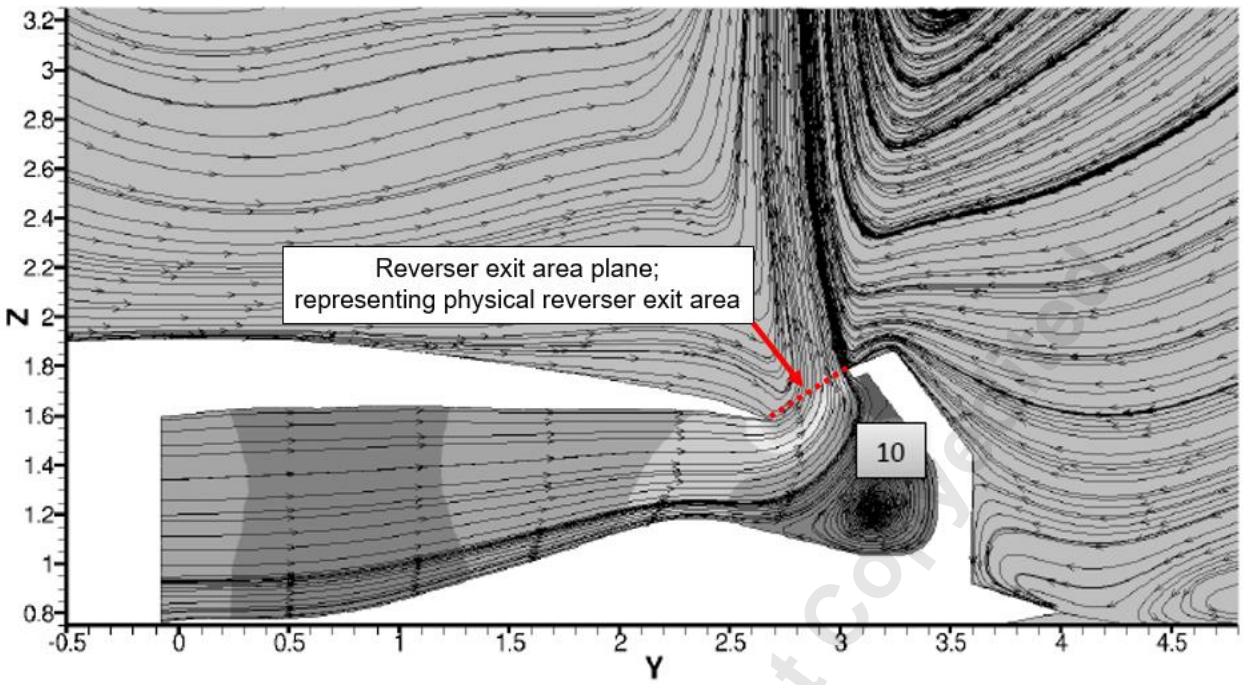

Fig. 7: (a) Shows the CMTTTR without kicker plate, (b) shows the CMTTTR with kicker plate; Kicker plate enhances the axial component of the reverse flow. In both designs, flow leave the TR exit area plane radially.

Reverser area ratio, (RAR), is defined as the ratio of *physical reverser exit area* to that of the *physical forward nozzle exit area* (i.e. A_{rev} / A_{fan}). In the experiment, three different RAR values were used i.e. 1.05, 1.15 and 1.25: all these configurations are tabulated in [Table 1]. The test results show all three RARs failed to satisfy the mass flow compatibility criteria [1]. This is mainly because the reverser door creates a blockage (zone 10, Fig 7) which reduces the reverser 'effective exit area'; the blockage and small effective reverser exit area also force the flow to turn at high angles around the bend and exit radially; see streamline plot in (Fig. 7).

Here, it is important to point out that in forward thrust configuration, the values of the bypass nozzle '*physical*' and '*effective*' throat areas are marginally different (as shown in Part 1) whereas, in the case of CMTTTR design, the values of '*physical*' and '*effective*' exit areas vary considerably (i.e. 'effective reverser exit area' is much smaller than the 'physical reverser exit area').

The CFD analyses are performed on configuration 7A and 8A: the only difference between these and test configurations 7 and 8 are the inclusion of the runway and wing [Table 1]. The RAR for both configurations is 1.25 and the reverser deployed angle is 40 degrees.

This paper also quantifies the influence of kicker plate on CMTTTR performance, hence, two dedicated engine CAD models are built, one with kicker plate and one without. The geometrical characteristics of the kicker plate are

the same as that used during the experiments. The overall size, location, installation and deployment angle (≈40°) of the CMTTTR is also the same for both the configurations (Fig. 3, 4 and 7) and is set as per the experiments in [1].

2.2 Mesh Generation

The Mesh generation process is similar to that carried out in Part 1, and only important considerations are outlined here to facilitate necessary understanding. Meshes for both the CAD models (i.e. with and without kicker plate) are generated using the ANSYS ICEM software; unstructured meshing is used on all parts. In comparison to Part 1, refined surface meshes are used for the TR deployed configurations; this is mainly because the flow analyses for the deployed reverser are far complex than that for the stowed configuration. A refined surface mesh is also constructed on the runway surface underneath the nacelle. Like Part 1, prism mesh comprises of 10 boundary layers. To fully capture the external flow physics, refined volume meshes are built around the following parts: CMTTTR, wing leading and trailing edges, nacelle inlet, and core nozzle exhaust; this is achieved by building Density blocks around these surfaces. Similar CFD studies were carried out for the cascade type reverser in ref [3] [4] and [5], and a clamshell type reverser in [6]. The CAD models in all these studies comprise of fuselage, wing, pylon and TR assembly. Unstructured meshing was used in all cases, and it was observed that approximately 5 - 6 million mesh elements are sufficient to satisfy the mesh sensitivity criteria. However, the CFD analyses performed in this paper found that approximately 8.1 million mesh elements are required to satisfy the mesh sensitivity criteria. One justification for the high number of mesh elements is that the studies in ref [3] [4] and [5] have used simplified versions of TR CAD models i.e. instead of using the actual CAD geometries for the cascade reverser blocks, Ref [3] [4] and [5] have simply drawn small rectangular surfaces on the outer nacelle. This means that no internal bypass and core sections were constructed, therefore the number of mesh elements must have reduced significantly. Although this approach may provide a reasonable view of the external flow fields, it is not adopted for this paper because the credibility of the mass flows exiting the reverser surfaces and velocity angles are questionable. Also, to measure the reverser performance, both the reverser stowed and reverser deployed analyses are necessary, and it is essential to observe the flow in the bypass region of the nacelle for the reasons already discussed in the last section. Also, refined surface and boundary layer meshes are built on the fan nacelle internal, external and TR surfaces, as static pressures will be measured and the values will be compared with the experimental data. Typical surface meshes are presented in Fig. 8-10.

Journal of Engineering for Gas Turbines and Power. Received August 17, 2017;
Accepted manuscript posted December 25, 2017. doi:10.1115/1.4038817

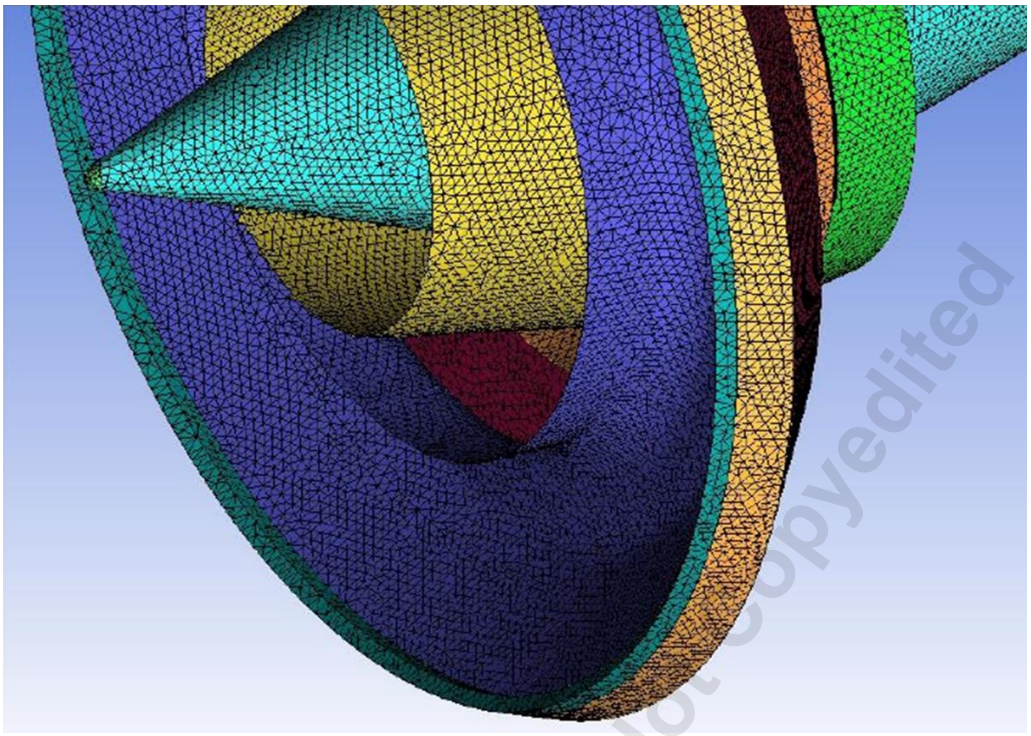

(8a) Surface meshes on the CMTTTR, kicker plate and exhaust plug.

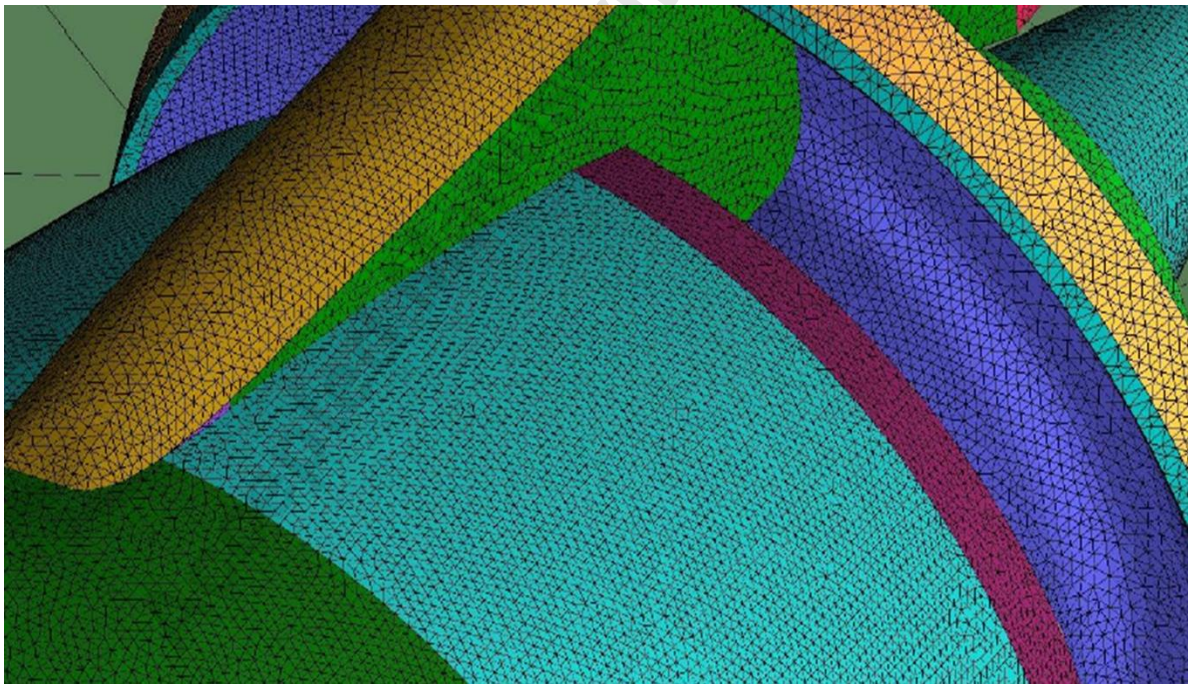

(8b) Surface meshes on pylon, nacelle, fan nozzle and CMTTTR.

Fig. 8: (a) Surface meshes on the CMTTTR, kicker plate and exhaust plug (b) Surface meshes on pylon, nacelle, fan nozzle and CMTTTR.

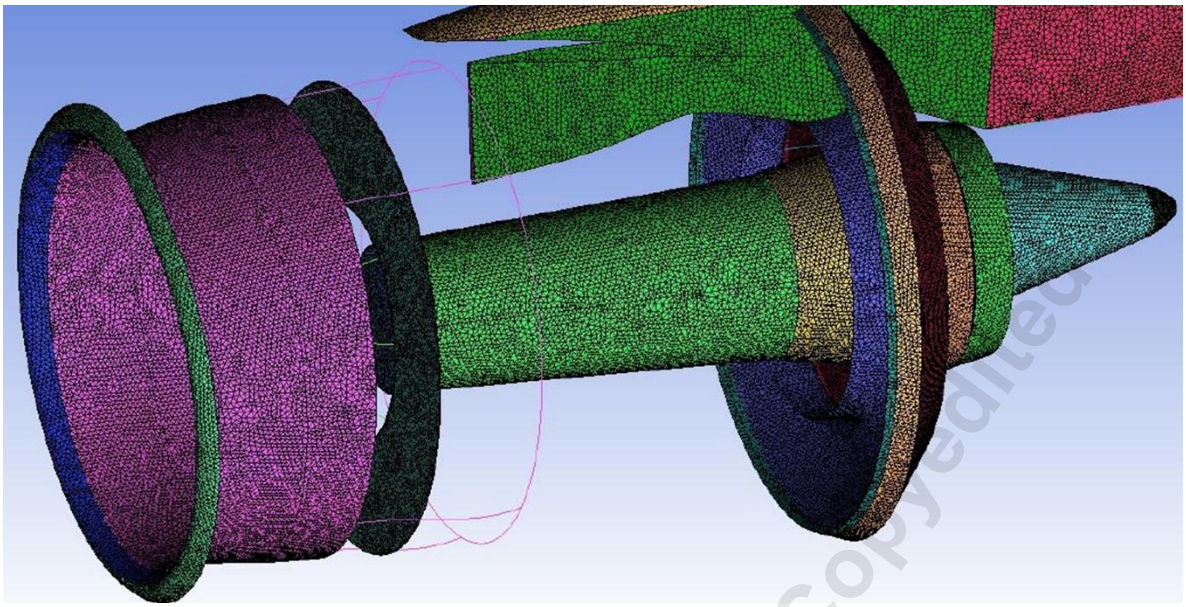

(9a) Surface meshes on core internal surface, pylon, core nozzle and exhaust plug.

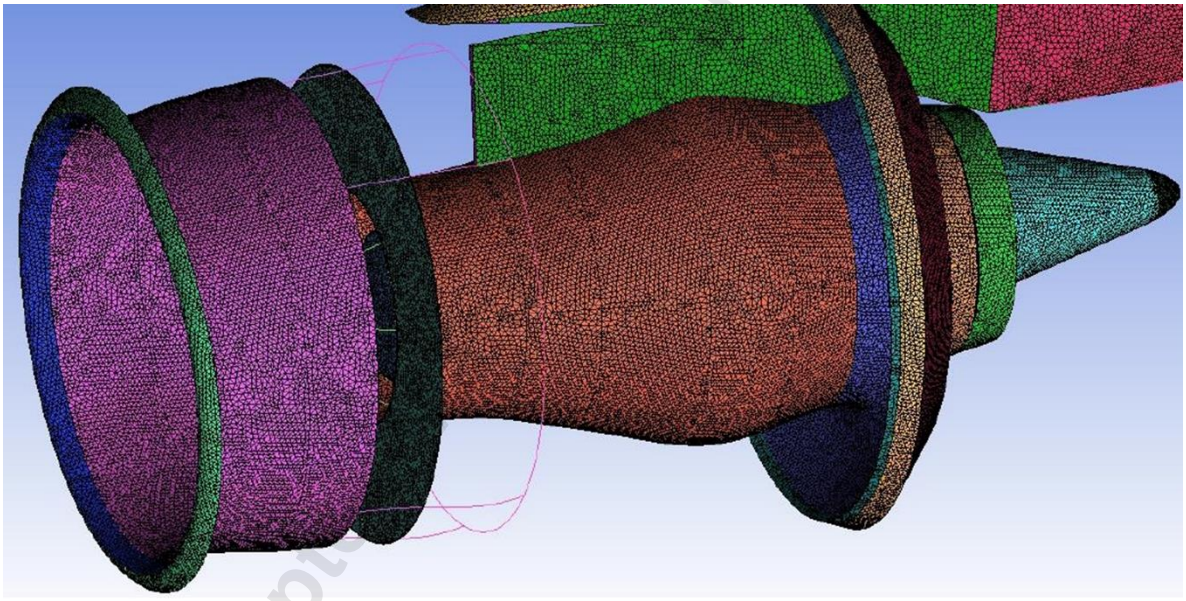

(9b) Surface meshes on core nacelle outer cowl.

(9c) Surface meshes on fan nacelle inner cowl and CMTTTR.

Fig. 9: (a) Surface meshes on core internal surface, pylon, core nozzle and exhaust plug, (b) surface meshes on core nacelle outer cowl, (c) surface meshes on fan nacelle inner cowl and CMTTTR.

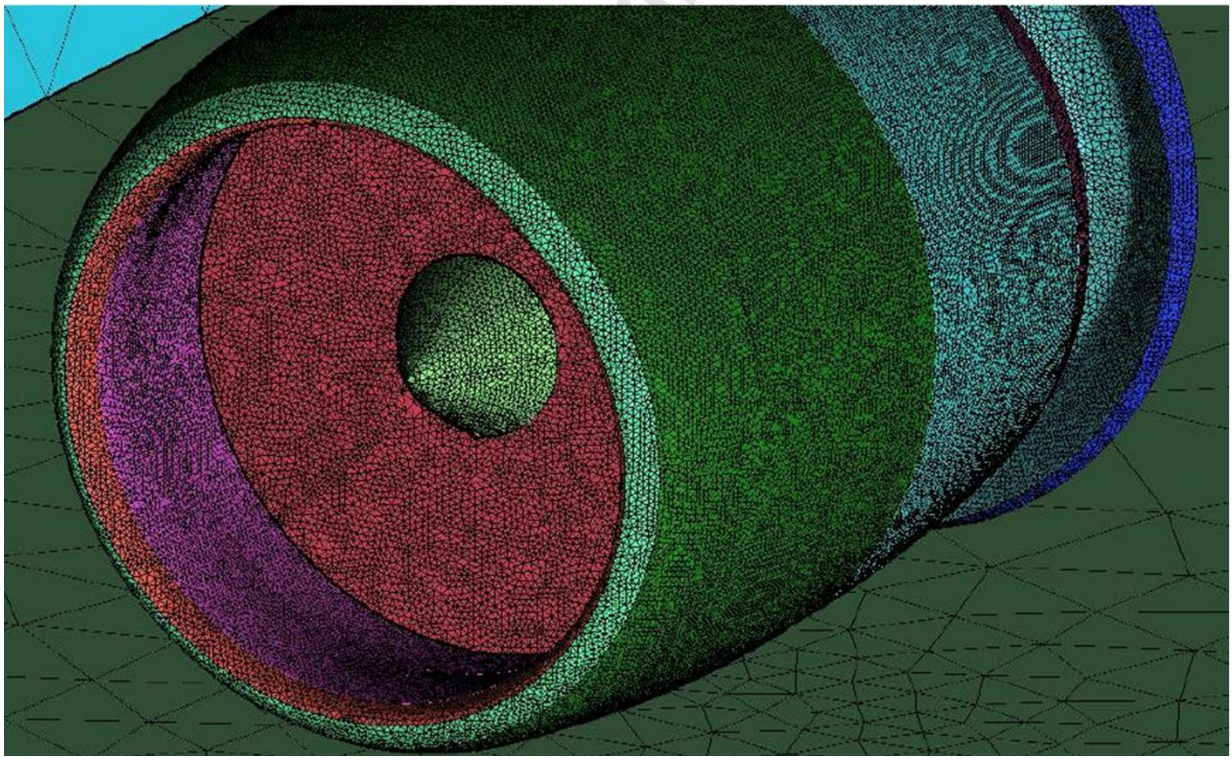

(10a) Surface meshes on engine inlet, nose cone, bypass nacelle, CMTTTR and runway.

Journal of Engineering for Gas Turbines and Power. Received August 17, 2017;
Accepted manuscript posted December 25, 2017. doi:10.1115/1.4038817

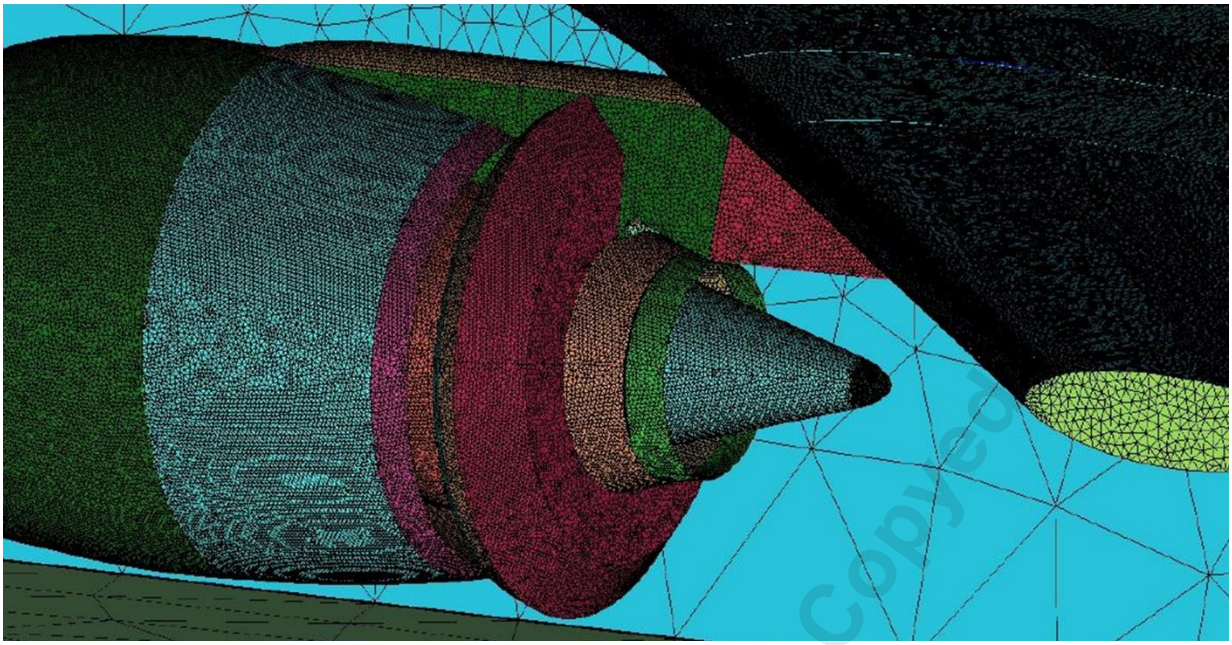

(10b) surface meshes on exhaust plug, pylon and wing.

Fig. 10: (a) Surface meshes on engine inlet, nose cone, bypass nacelle, CMTTTR and runway. (b) surface meshes on exhaust plug, pylon and wing.

2.3 CFD Setup

The authors have thoroughly reported on the CFD setup in Part 1 of this paper, therefore to avoid repetition, only relevant and important considerations are highlighted herein. Commercially available software, FLUENT [7] is employed for the implementation of the CFD analyses. Pressure based solver, with segregated algorithm was selected and applied, which solves the governing equations sequentially [7]. The preferred turbulence model to support the analyses was k-ε realizable; it is best suited for applications where separation and complex secondary flow features are found; previous studies carried out in academia and industry have also employed the same model [3] [4] [5]. Second order upwind scheme is used for all the variables; in it, the higher order accuracy is achieved at cell faces through a Taylor series expansion of the cell-centered solution about the cell centroid [7].

Air with ideal gas properties is selected as the working fluid. The convergence is observed by making sure that the second order residuals remain unchanged; it is ensured that the mass, momentum, and energy residuals are less than 10^{-4}. A mass flow balance criterion is also established for each case; this is achieved by calculating the mass flows for bypass and core streams at inlets and nozzle exits.

To setup the boundary conditions in FLUENT, values of pressure and temperature are required for fan inlet, fan outlet and core inlet surfaces: all these values are obtained from the engine performance study. The far field boundary conditions are set at an ambient pressure of 101325 Pa, and ambient temperature=288K.

2.4 Engine Performance Data Acquisition

Part 1 of this paper provides a detailed explanation on the importance of the engine performance data and how it is used to setup boundary conditions in CFD simulations. The interested reader is therefore encouraged to read relevant sections in part 1 to facilitate greater understanding.

The CFD boundary conditions for the reverser deployed configuration are obtained from the engine off-design study (see Table in Part 1). The main difference between this off-design study and that carried out in Part 1 is that the fan nozzle throat area is 1.25 times larger than that at design point.

In the experiments, CMTTTR performance was measured for FNPRs as high as 2.0 [1]; however, for the CFD analyses the maximum value of the FNPR ratio is restricted to 1.57. This is because CUTS_TF is a high bypass ratio engine (i.e. BPR≈9), and considering the aircraft is at sea level with TR deployed, values of FNPR higher than 1.57 are not practical.

It is interesting to note that the CFD analyses in Ref [3], [4] [5] and [6], have not mentioned the source of the performance data, nor was there any concrete discussion on how this data was generated and what software's were used. No justification was provided as to why the boundary conditions they have used are appropriate. The authors believe that without a good and credible set of engine performance data, the boundary conditions for the CFD analyses may be questionable, especially if the reverser performance needs to be measured.

3. RESULTS AND DISCUSSION

3.1 Validation of CFD Data

NASA carried out extensive testing of CMTTTR in deployed configuration. Experiments at static conditions were run for a range of FNPRs. Static pressure values were recorded on the core external (i.e. PSIFD1-10), fan nacelle internal (i.e. PSOFD1-5), fan nozzle internal (i.e. PSFEN1-4), pylon (i.e. PSPYL1-5) and CMTTTR internal surfaces (i.e. PSATR1-4); all values were measured at 14 degrees clockwise from the engine centerline, as shown in (Fig. 11).

Journal of Engineering for Gas Turbines and Power. Received August 17, 2017;
Accepted manuscript posted December 25, 2017. doi:10.1115/1.4038817

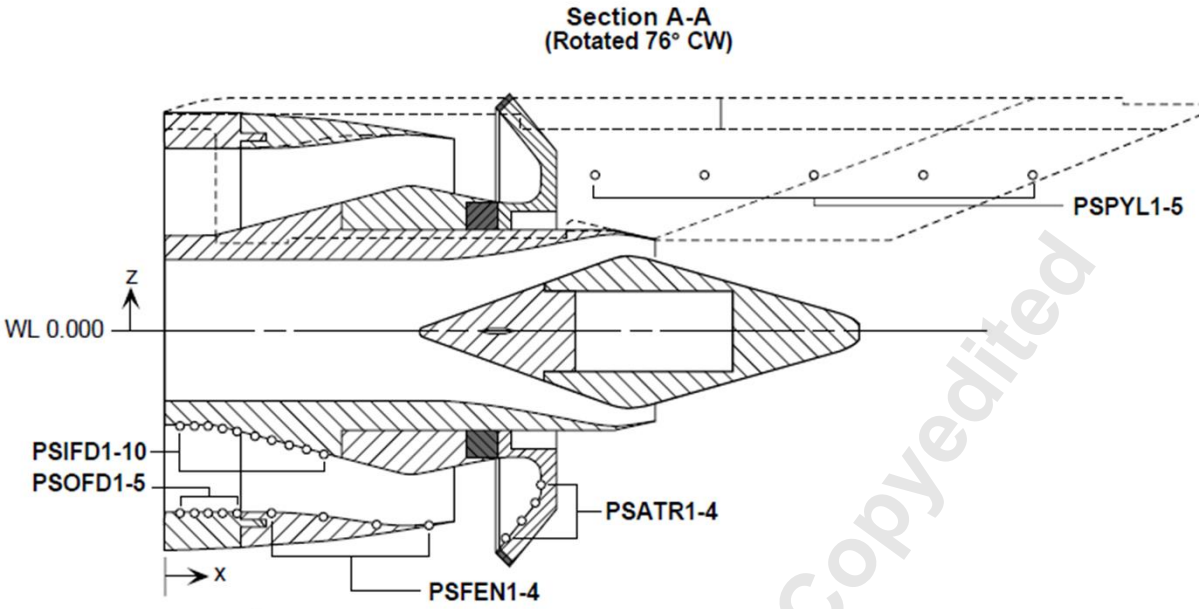

Fig. 11: Locations where static pressure measurements were recorded during experiment [1].

Availability of the experimental data is a very useful source, and this data is used for validating the CFD results. The static pressure values obtained from the CFD analyses are compared with the test data for the following two configurations:

i) CMTTTR deployed at 40 degrees, RAR=1.25, No kicker plate

ii) CMTTTR deployed at 40 degrees, RAR=1.25, with kicker plate.

It is evident from Figs. 12-13 that the results acquired from the CFD analyses exhibit good agreement with the experimental data. If static pressure readings at fan nacelle internal and core external surfaces are compared, then the approximate difference between experiments and CFD results is about 2%. However, for the target reverser internal surface, the difference is more than 2%. This may be because reverser deployment causes the flow to take a sharp turn towards the reverser exit and in this process a re-circulating vortex is formed (Fig. 7); in authors' view, it is difficult to take accurate measurements within this re-circulating vortex. Figure 13 shows this difference has increased further with kicker plate, mainly because the turning radius has reduced, causing the flow to accelerate along the kicker surface (Fig. 7); this, in turn, increases the momentum of the re-circulating vortex.

Journal of Engineering for Gas Turbines and Power. Received August 17, 2017;
Accepted manuscript posted December 25, 2017. doi:10.1115/1.4038817

Part 1 of this paper addressed reasons for discrepancies between experiment and CFD; they are also applicable here. The static pressure values for pylon are not validated against the experiment, as the tests were carried out without a wing, whereas CFD analyses are performed with the wing.

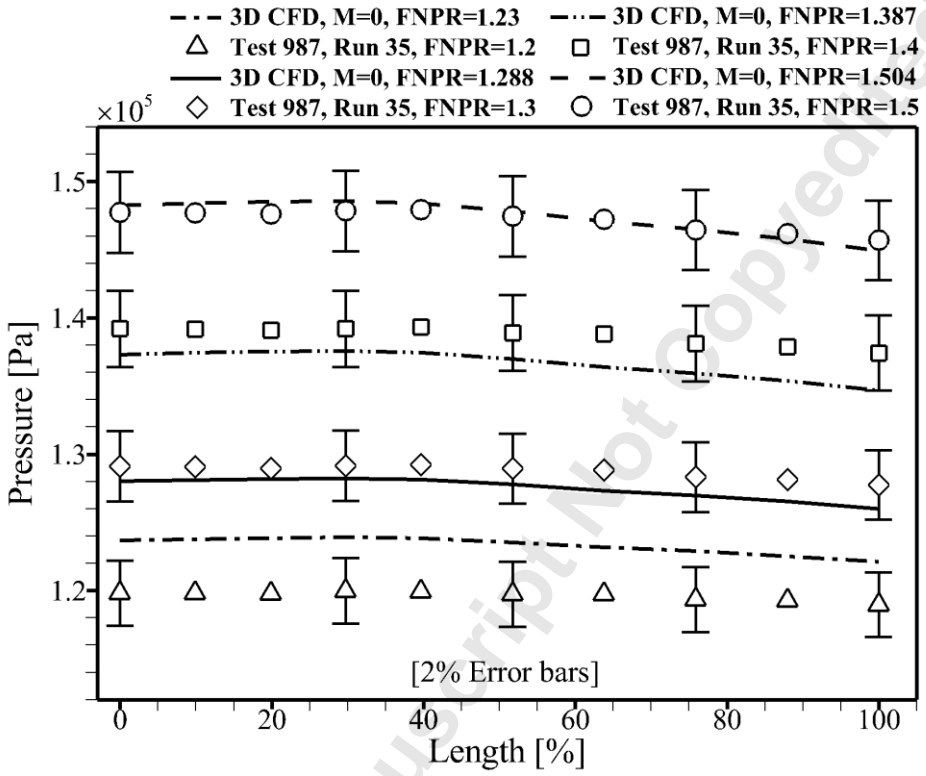

(12a): Core nacelle internal surface

Journal of Engineering for Gas Turbines and Power. Received August 17, 2017;
Accepted manuscript posted December 25, 2017. doi:10.1115/1.4038817

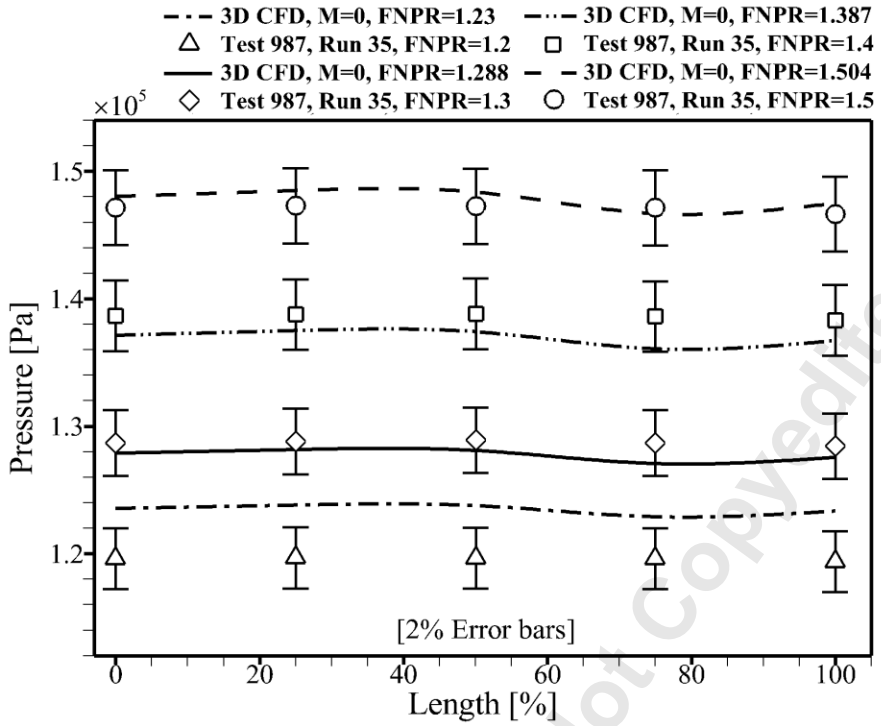

(12b) Fan nacelle internal surface

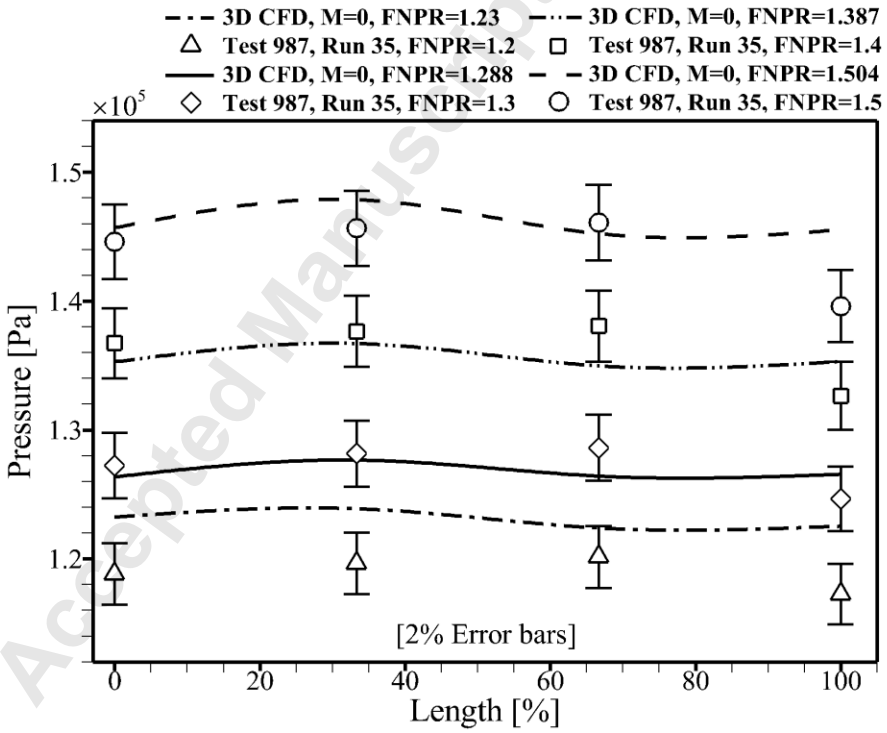

(12c) reverser internal surface.

Fig. 12: Comparing CFD results with test data. Reverser is deployed, no kicker plate installed. (a): Core nacelle internal surface, (b) Fan nacelle internal surface and (c) reverser internal surface.

Journal of Engineering for Gas Turbines and Power. Received August 17, 2017;
Accepted manuscript posted December 25, 2017. doi:10.1115/1.4038817

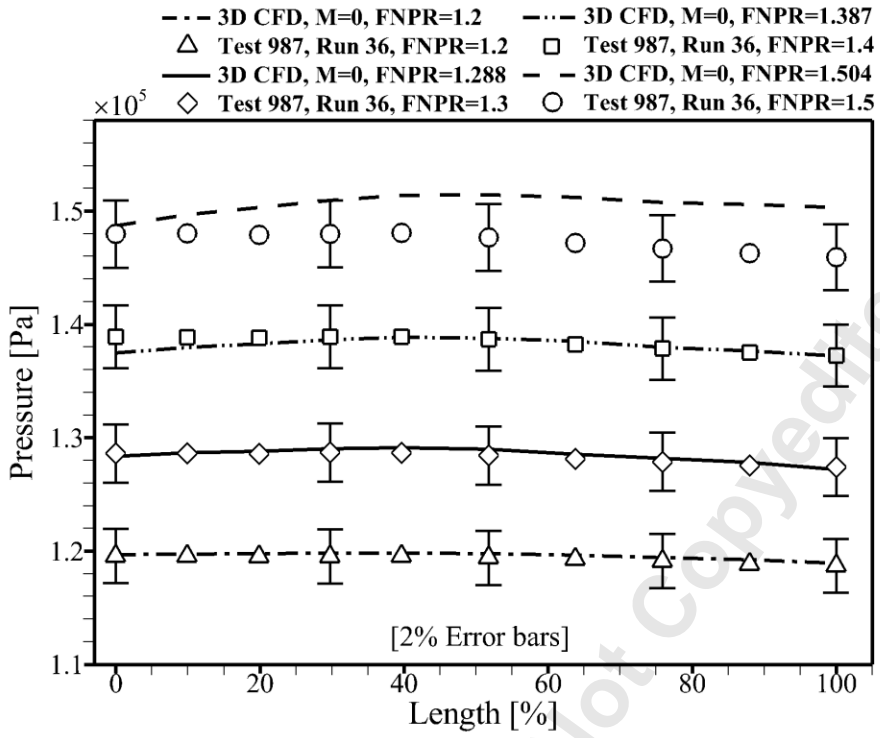

(13a): Core nacelle internal surface

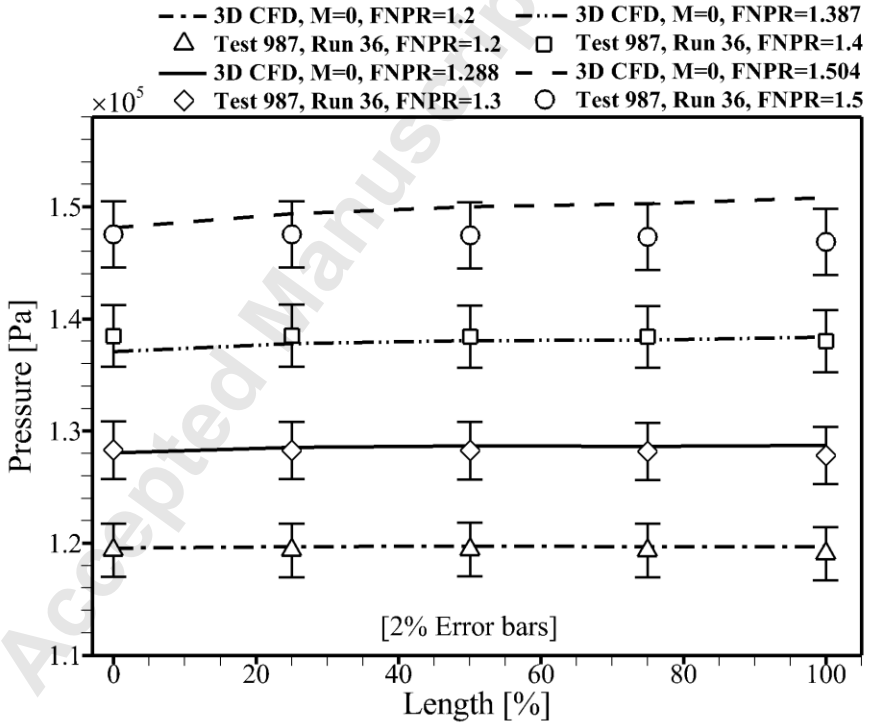

(13b) Fan nacelle internal surface

Journal of Engineering for Gas Turbines and Power. Received August 17, 2017;
Accepted manuscript posted December 25, 2017. doi:10.1115/1.4038817

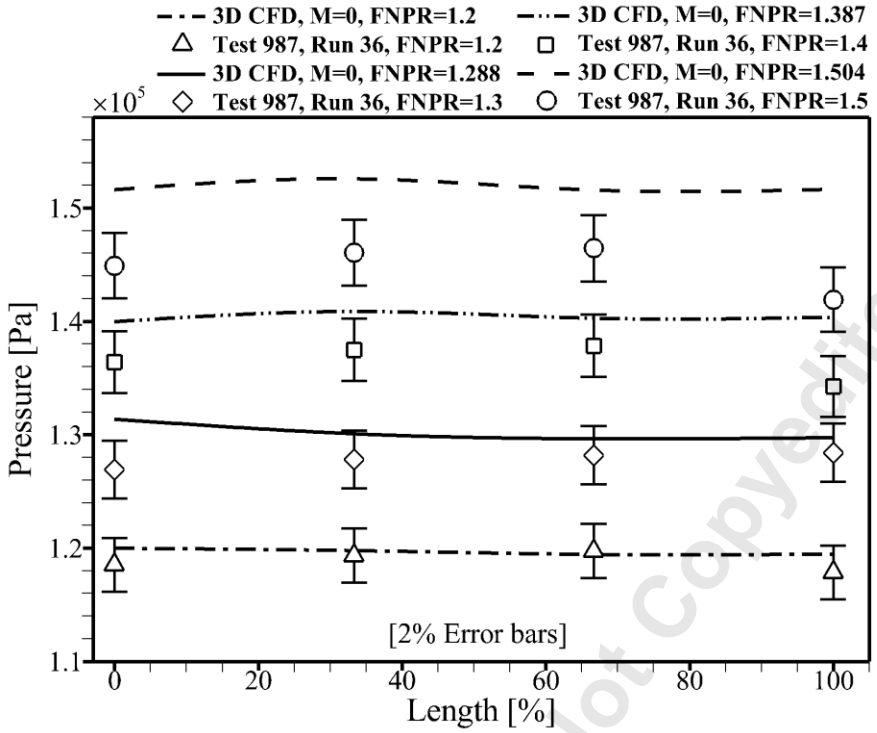

(13c) reverser internal surface

Fig. 13: Comparing CFD results with test data. Reverser is deployed, kicker plate installed. (a): Core nacelle internal surface, (b) Fan nacelle internal surface and (c) reverser internal surface.

3.2 Estimation of Reverse Thrust

The total gross thrust on a high bypass ratio turbofan engine is the sum of thrust produced by the bypass and core streams. The exhaust flow from the bypass and core nozzles is mainly axial, and hence the gross thrust can also be referred as an axial thrust or F_A (i.e. thrust in the x-direction). However, when a TR on a HBPR engine is deployed, the presence of the blocker doors will re-direct the bypass flow through the reverser exit, mainly using the target surfaces (Fig. 1 and 7). The flow through the reverser will no longer be axial; strictly speaking, it will be three-dimensional. The resultant thrust produced by the bypass stream will have X, Y and Z components i.e. F_X (axial), F_Y (radial), F_Z (side-force) components. The resultant thrust will thus be represented by the following equation:

$$F_{Resultant\ thrust,\ Thrust/Rev\ Deployed} = \sqrt{F_X{}^2 + F_Y{}^2 + F_Z{}^2} \qquad \text{(Eq. 1)}$$

In a well-designed TR, component F_X will approximately be ≈ 40%. Another important design requirement for the flow is to exit the TR such that it will travel in the direction opposite to the free-stream (i.e. towards the engine front). The value of F_Y (i.e. vertical/radial component of reverse thrust) will also be present; however, in a well-designed TR this vertical thrust will be relatively small so as to minimize interference with the wing and ground. F_Z

is the side force component, this will be lowest in magnitude, and in a well-designed reverser most of this will cancel due to symmetry.

The performance of a TR is usually measured by its effectiveness; the two most common reverser effectiveness equations are:

i) Fan reverser effectiveness:

$$\eta_{Fan} = \frac{F_{rev}}{F_{fan}} \quad \text{(Eq. 2)}$$

In Equation 2, F_{rev}, is the gross reverse thrust, it is defined as the sum of the reverse thrust axial component, F_X, and the engine core thrust during reverser deployment, $F_{core,\,Thrust/Rev\,Deployed}$. It is important to measure the core thrust in reverser deployed condition: this core thrust value will be different from that measured in reverser stowed configuration because it is affected by the external flow field. The value of F_X can either be positive or negative; it is important to ensure that the correct sign is used. If the reverse flow is travelling in the direction opposite to core flow (i.e. producing reverse thrust) then a negative sign is used; however, in case the TR is designed poorly and F_X is in the same direction as the core flow then a positive sign will be used.

$$F_{rev} = F_X + F_{Core\,Thrust,\ \ Rev\,Deployed} \quad \text{(Eq. 3)}$$

F_{fan}, in Equation 2, is the fan nozzle forward thrust, as calculated in Part 1 [2].

ii) Overall reverser effectiveness:

$$\eta_{rev} = \frac{F_X}{F_{Total\,Fwd\,Thrust}} \quad \text{(Eq. 4)}$$

In Equation 4, F_X, is the reverse flow axial component and is the same as defined in Equation 1 and 3. F_{Total}, on the other hand, is the total forward thrust (i.e. $F_{Fan} + F_{Core}$), defined as the sum of fan nozzle and core nozzles forward thrust, which is already calculated in Part 1 [2].

It is evident from (Eq. 1-4) that estimation of reverser performance also requires data from the forward flight condition. Engine performance data such as: thrust, mass flows, exhaust velocities, nozzle areas, and static pressure values at forward flight condition are all essential, as otherwise calculating the reverser effectiveness is not possible. This shows the importance of the exercise conducted in Part 1 [2]. Equations 1–4, are the same as that used by NASA for reverser performance estimation [1].

During experiments [1], CMTTTR overall reverser effectiveness, η_{rev}, was measured for a range of FNPRs; these values are compared here against the data obtained from the CFD study, as shown in Fig. 14. Engineering data from

both Part 1 and Part 2 are used for the estimation of overall reverser effectiveness. The results for both the CMTTTR designs (i.e. with and without kicker plate) are presented in Fig 14. The results from the experiment shows that the both the CMTTTR designs are not promising, and the overall reverser effectiveness for each design is less than 10%. The results from CFD analyses shows a good agreement with experiment data, however, it is noted from the CFD analyses that the reverser axial component, F_X, is in fact producing forward thrust (i.e. the axial force vector is in the direction of core flow). This is contrary to the results presented by NASA, which may be due to any one or the combination of the following reasons:

1. It is stated in [1] that a six-component strain gauge was used to measure the moment and forces; however, the actual method used in estimating the reverser force components (i.e. F_X, F_Y, F_Z,) is not described in detail; the authors believe that measuring the X, Y and Z velocities at the reverser exit is not practical in the experiment. Also, there is no mention of the likely percentage errors associated with the measuring instruments. However, in the CFD analyses, the reverse thrust is measured on the exit plane between the reverser and the nozzle, as depicted in Fig. 7.
2. Although the CFD results shows that the reverser is contributing to forward thrust the difference between the experimental and CFD values is less than 10%, and this small difference may be due to turbulence models used in the CFD study.
3. The difference could also be due to small geometric tolerances such as reverse exit area, target angle, nozzle internal surface, or perhaps may be due to the installation of a wing, as in the experiments no wing was included.
4. The boundary conditions used in the CFD analyses may be slightly different from that used during the experiments. The boundary conditions in the CFD analyses are obtained from the engine performance study (i.e. Part 1[2]); values of static pressure may be slightly different from that used during the experiments, whereas the values of static temperature may be considerably different, as during experiments air temperature is not varied; whereas in the CFD study a new value of static temperature is used for every other FNPR. These differences in boundary conditions may be the reason for the small variation in results between experiment and CFD analyses.

Journal of Engineering for Gas Turbines and Power. Received August 17, 2017;
Accepted manuscript posted December 25, 2017. doi:10.1115/1.4038817

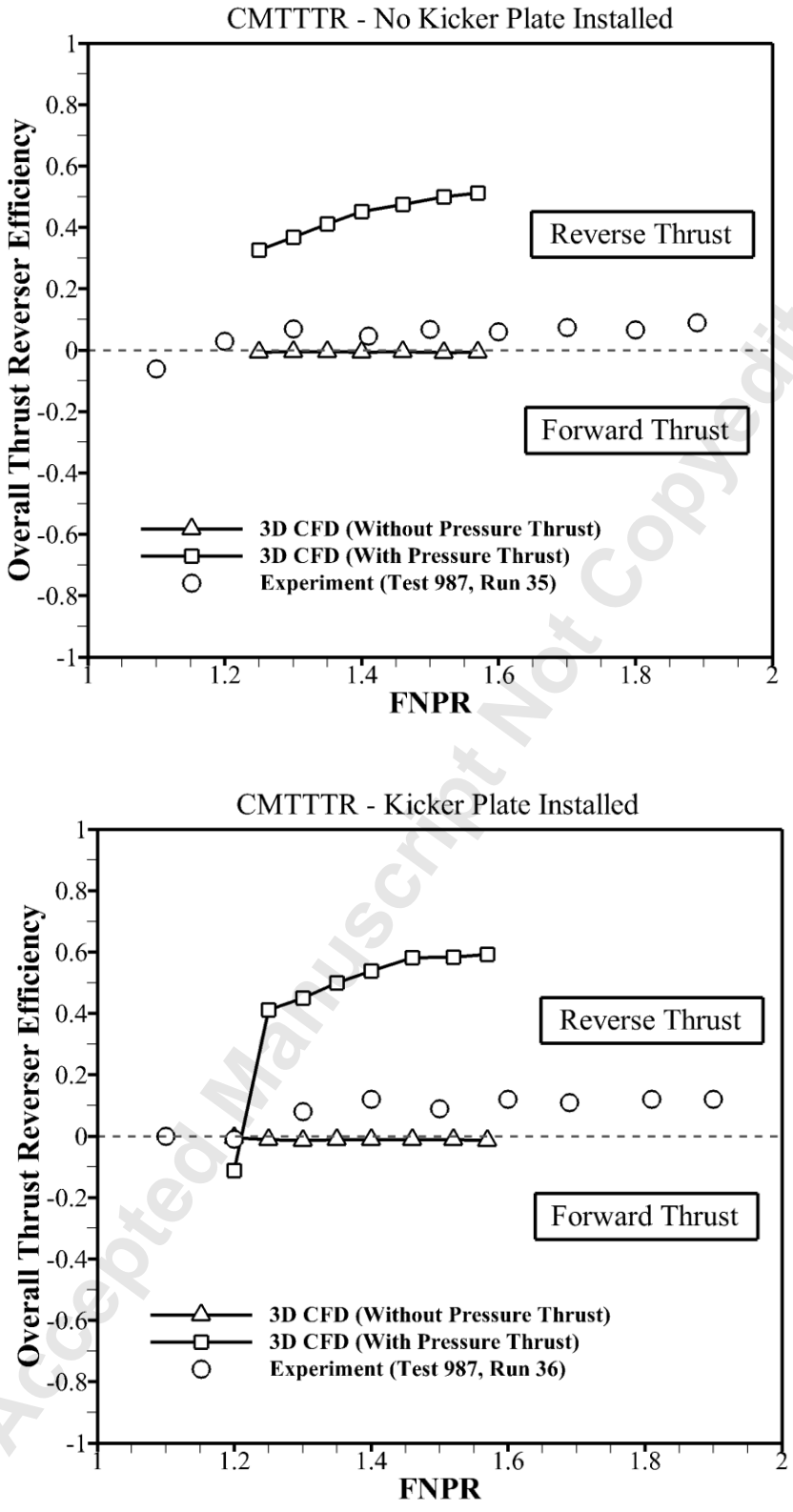

Fig. 14: Comparison of test and CFD results for Overall Thrust Reverser Effectiveness. (a) No kicker plate installed. (b) Kicker plate installed. Also, shown on the figure is the increase in overall reverser effectiveness when the pressure thrust is included in the CFD results.

Table 1 shows that although the area ratio for the both the CMTTTR designs is approximately 1.25, the effective reverser exit area for the CMTTTR is significantly less than that for the forward thrust configuration (see Fig. 7). In a well-designed TR, the mass flow ratio should ideally be around 1.05 or close to 1.0; however, with the CMTTTR design it is approximately 0.6 [Table 2] this means that the cold stream mass flow during reverse thrust operation is reduced by 40%, which is mainly due to the reduction in reverser exit area.

In a well-designed TR, axial force component, $F_{X,}$ must be maximum: however, with the CMTTTR design it is observed that the radial force component, F_Y, is the largest as tabulated in [Table 2]. Thus, the CMTTTR design is not satisfactory as the main objective of any TR is to produce reverse thrust and not the radial thrust.

Another observation of the CMTTTR design is the unbalanced radial force. Generally, in HBPR pod-mounted engines, TR designer takes advantage of symmetry and the TR is designed such that the radial forces generated in the top and bottom half of the reverser cancel each other; in a cascade type thrust reverser this is usually achieved by installing a blocker in the bottom half of the TR: the solid block is usually in line with the pylon. However, in the case of CMTTTR design, the reverser exit areas in the top and bottom half of the reversers are not equal, because the pylon is installed in the top section; therefore, there is no blockage to compensate the effect of pylon in the bottom half of the reverser, which results in the bottom half of the reverser having a larger reverser exit area. Furthermore, in the experiments the top and bottom half of the engine nacelle and TR geometries are symmetric, whereas the engine CAD model used for the CFD analyses is not completely symmetric. As previously mentioned in Part 1, the bottom half of the external nacelle has a larger curvature: this is because it needs to accommodate a large gear box, and also it is designed such as to avoid flow ingestion and F.O.D problems during landing. Therefore, a significantly high net radial thrust is generated. The direction of this resultant vertical force is such that it will generate an unbalanced upward force on the aircraft, which will be detrimental during landing; as it could compromise the surface contact between the aircraft and the runway, and thus, additional decelerating force may be required from the aircraft wheel braking mechanism and lift spoilers.

The side force component, F_Z, is also measured: however, the value of this force is very small, and the majority of this force cancels out due to symmetry.

Overall, it is observed that the CMTTTR design failed to produce any noticeable reverse thrust because reverser effectiveness falls significantly short of the standard 40% mark. The only noticeable force that is generated from the CMTTTR design is in the radial direction.

3.3 Importance of Pressure Thrust

Each time a pivoting or target type thrust reverser is deployed; the reverser frontal and rear faces are likely to be at a different pressure (Fig. 15). The difference in pressure between the two faces will generate an additional decelerating force, which in this paper is referred to as the 'Pressure Thrust' or $F_{Pressure\ Thrust}$, (i.e. a decelerating force due to the pressure difference across the TR surfaces). The resultant, $F_{Pressure\ Thrust}$, force will act axially; if this force is added to F_X, a revised equation for overall thrust reverser effectiveness, $\eta_{rev,2}$ is obtained, as expressed in Equation. 5.

$$\eta_{rev,2} = \frac{F_{Pressure\ Thrust} + F_X}{F_{Total}} \quad \text{(Eq. 5)}$$

The authors are therefore proposing another equation for total decelerating force during reverser deployment:

$$F_{Total,Decelerating\ Thrust} = F_{Momentum\ Drag} + F_{Pressure\ Thrust} + F_X - F_{Core\ Thrust,Rev\ Deployed} \quad \text{(Eq. 6)}$$

In the above equation, $F_{Momentum\ Drag}$ will be zero if the aircraft is stationary. F_X is positive if the reverser generates reverse thrust: if no reverser thrust is generated, the sign for F_X will be negative.

As per the information available in public domain, no previous study has highlighted the importance of estimating pressure thrust, neither has anyone ever proposed Equation 5 and 6. Both these equations are important and they should be used in estimating reverser effectiveness and performance.

From the CFD analyses, it is found that the pressure thrust is significantly large in magnitude and should not be ignored (Fig 15). The results are presented in Table 2 and Fig. 14. Equation 5 is suitable for all types of thrust reversers i.e. pivoting door, target type, and cascade type thrust reversers. With cascade type reverser, $F_{Pressure\ Thrust}$ is estimated around the blocker door.

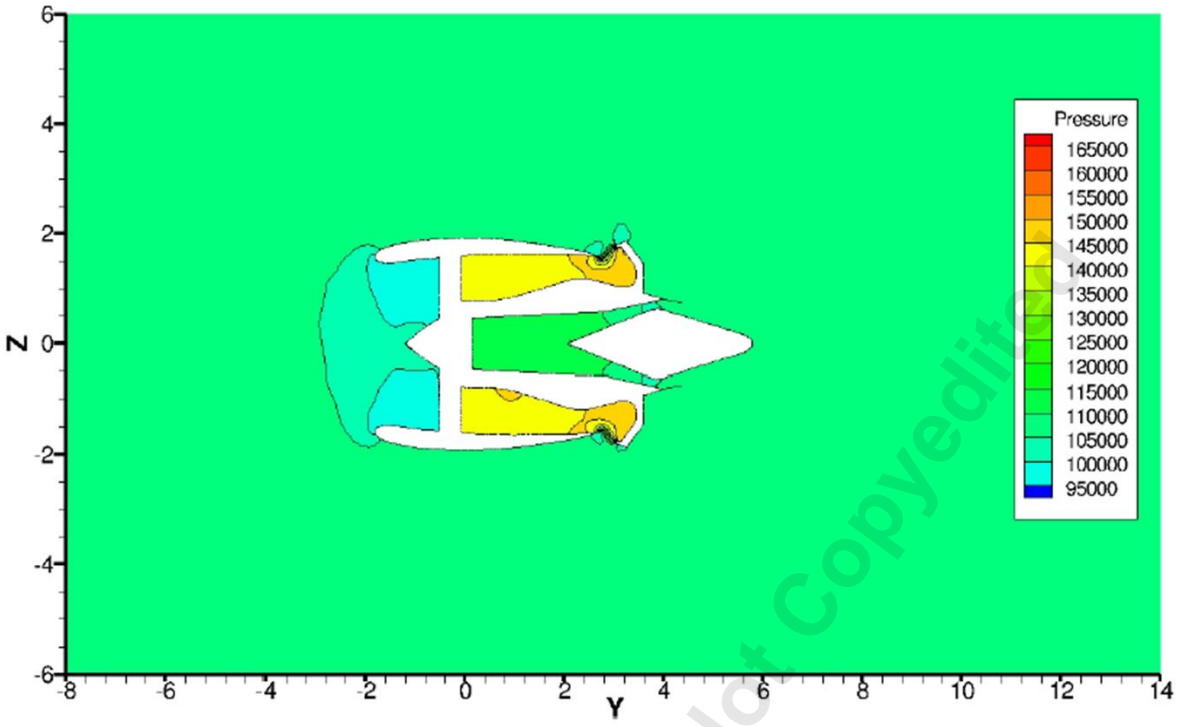

Fig. 15: Static pressure contours on a 40 degree CMTTTR, M=0.0, FNPR=1.45. Kicker plate installed.

3.4 Importance of Kicker Plate

In most of the pivoting and target type thrust reversers, kicker plate is integrated on the outer periphery of the reverser surface (Fig. 2, 4, 7 and 8). Installation of kicker plates on TRs is not new and has been around for many years. Its purpose is of course to enhance the performance of the axial component of reverse thrust i.e. F_X.

From the CFD analyses, it is found that the kicker plate will, in fact, enhance the performance of the CMTTTR. This is achieved in two ways. First, it is noticed that the installation of a kicker plate will enhance the reverse thrust axial component, F_X, (Table 2). The second and more intriguing fact is that the kicker plates affect pressure thrust values; it is noticed from the CFD analyses that installation of a kicker plate increases pressure thrust, $F_{Pressure\ Thrust}$. This additional decelerating force will be beneficial, especially in critical conditions where the runway is wet or icy, or where the pilot needs to abort the take-off.

Table 2: Results obtained from the 3D CFD Analyses

No	$FNPR$	$\frac{\dot{W}_{Rev,Thrust}}{\dot{W}_{Fwd,Thrust}}$	$F_{Fan\ Fwd}$ (KN)	$F_{Forward,\ Thrust}$ (KN)	F_X (KN)	F_Y (KN)	F_Z (KN)	$F_{Core\ Thrust\ Rev\ Deployed}$ (KN)	$F_{Resultant,\ Thrust}$ (KN)	$F_{Pressure\ Thrust}$ (KN)	$F_{Total\ Decelerating,\ Thrust}$ (KN)	η_{Fan}	η_{rev}	$\eta_{rev,2}$
40 Degree CMTTTR without a Kicker Plate at M=0.0														
1	1.25	0.57	163.3	173.4	1.13	33.5	0.01	5.2	33.5	57.7	51.4	0.04	0.01	0.33
2	1.35	0.58	219.6	235.8	1.28	45.5	0.01	7.7	45.5	98.4	89.4	0.04	0.01	0.41
3	1.45	0.60	280.8	311.7	1.54	60.2	0.03	11.2	60.2	149.6	136.8	0.05	0.01	0.47
4	1.57	0.62	342.2	395.3	2.65	73.7	0.09	15.7	73.7	205.1	186.7	0.05	0.01	0.51
40 Degree CMTTTR with Kicker Plate at M=0.0														
1	1.25	0.6	163.3	173.4	1.85	33.5	0.01	5.2	33.6	73.6	67.7	0.04	0.01	0.44
2	1.35	0.6	219.6	235.8	2.75	37.7	0.01	6.9	37.8	98.5	91.5	0.04	0.01	0.43
3	1.45	0.6	280.8	311.7	3.61	65.7	0.03	11.3	65.8	184.8	173.4	0.05	0.01	0.60
4	1.57	0.6	342.2	395.3	5.51	69.7	0.09	16.0	69.9	239.7	223.5	0.06	0.01	0.62

3.5 Analyses of CMTTTR in Deployed Configuration

In this section, flow analyses of the CMTTTR in deployed configuration are discussed. During this study, several CFD analyses are carried out to assess the performance of the CMTTTR at different thrust settings, and it is observed that at each thrust setting, the external flow characteristics of the CMTTTR will be different. However, discussing the reverser flow characteristics at every FNPR value will be a study in its own right, and therefore herein only the discussion analyzing the flow characteristics at the maximum reverse thrust condition i.e. (FNPR≈1.57) is elaborated.

Flow visualization of the 3D model is presented in Fig. 18. However, to understand the flow behaviour in greater detail, horizontal and vertical streamlines plots are constructed about engine centre line Figs. 16-17. The acquired streamline plots are for the condition corresponding to FNPR≈1.57. In order to further support the understanding of the reverser flow physics, the flow in the horizontal and vertical streamline plots are divided into 21 zones; 12 zones corresponding to the flow in horizontal plane as highlighted in Fig.16, and the remaining 9 zones correspond to the flow behavior in the vertical plane as highlighted in Fig. 17. The following sections will elaborate on each plane respectively.

3.6 Flow behavior of the CMTTTR as seen on the horizontal plane from the engine center line

This section discusses the flow characteristics of the CMTTTR in the horizontal plane. Two streamline plots are presented in Fig. 16; the top plot represents the flow behavior in the wider domain and the bottom plot is a magnified image of the first and represents the reverser flow characteristics in the immediate vicinity of the engine.

The flow characteristics in the upper half of Fig. 16 are divided into four different zones. The area upstream of the engine is referred to as zone 1. It is observed that at static conditions, a major portion of the reverser exhaust flow will travel upstream and as the flow is coming from both sides (i.e. port and starboard) of the nacelle. Part of this flow will enter the engine inlet, and the remaining part of the flow will meet at approximately 5m ahead of the engine, at which point the streamlines will become uniform and the flow will continue to travel upstream. Interestingly, this shows that it is advisable that the thrust reverser must be designed such that the reverser exhaust flow will have minimal impact on the engine intake flow.

The flow region on the port side (i.e. right side if looking from the front of the engine) of the nacelle is represented by zone 2. The outer boundary of zone 2 starts where the reverser high momentum vortex ends which is approximately some 10m from the engine centre line, as shown in Fig. 16. The streamline behavior in zone 2 creates a D-shape; this

D shape region has two prominent left and right boundaries. The flow boundary on the left-hand side of Zone 2 is created due to the high pressure, high momentum reverser exhaust flow and the right-hand boundary is formed due to the high momentum core flow entraining the surrounding atmosphere; between these two boundaries, a large anti-clockwise re-circulating vortex will form which is represented by zone 2.

Zone 3, represents the external flow field between zone 2 and zone 4 (Fig. 16); the flow in this region is mainly subsonic and the streamline plot shows that the flow will travel inwards towards the core flow. The shape of the streamlines in this region is thrust dependent.

The flow field in Zone 4 is also thrust dependent. At higher thrust settings, the exhaust flow will have high momentum and will continue to travel straight. It is interesting to note that the symmetry boundary condition will have an influence on the core exhaust flow. Figure 16 shows that the flow in zone 4 deflects toward the aircraft centre line. This means that flow on either side of the aircraft centerline will eventually merge at some distance downstream. However, at low power the momentum of the core exhaust flow will reduce and is susceptible to the reverser exhaust flow; there exists a possibility that some distance downstream, the aft flow field created by the reverser exhaust may affect the momentum of the core flow, and the core flow may end up having additional re-circulating vortices.

The bottom half of Fig. 16 shows an enlarged picture of CMTTTR where zone 10 represents a re-circulating vortex. It is observed that as the bypass flow approaches the reverser exit, a clockwise re-circulating vortex will form between the core outer cowl and the reverser inner surface, depicted in Fig. 7. The formation of this clockwise re-circulating vortex is the main source of blockage, and will generate an adverse effect on the fan outlet mass flow; after the vortex, the streamlines travel in the vertical upward, and downward direction.

The deployment of a CMTTTR will result in the formation of three large re-circulating vortices; two of the counter-rotating vortices will form on the starboard side (i.e. left side if looking from the front of the engine) or towards the aircraft centerline (i.e. zone 7 and 9), and a single vortex will form on the port side identified as zone 8. At static conditions, these vortices can be as much as 2.5 times the engine size. The reason for the formation of two counter-rotating vortices (i.e. zone 7 and 9) on the starboard side is due to the symmetric boundary condition, which assumes that there is an engine on either side of the symmetry. When the flow from the two reversers approaches each other, a stagnation point will form, which results in the formation of two contra-rotating vortices. Also, the gap between the two engines is fixed as per the aircraft design, which results in the formation of a flow passage; the size of this flow passage along with the free stream boundary conditions will affect the strength, size and characteristics of these

vortices. It is important to note that even if the wing was integrated onto the fuselage, it would have still resulted in the formation of two contra-rotating vortices in zone 7 and 9.

On the port side of the streamline plot, there is no obstruction; the flow leaves zone 10 in the port-wise direction and forms a natural clockwise vortex. The formation of this clockwise vortex, as shown in zone 8, is due to the momentum difference between zone 10 and 6. Part of the flow from zones 7 and 8 will travel upstream, towards the engine inlet, forming zone 5 and 6, which as previously discussed will introduce flow ingestion and give rise to distortion. High momentum flow in Zone 8 will also affect the far field flows in zone 2 and zone 3, which is discussed previously.

Kicker plate is an important design feature; CFD analyses (i.e. Fig. 7) shows that kicker plate can help improving the reverser performance by enhancing the axial component of the reverser flow. The flow will experience more favourable deflection with kicker plate than without. The upper half of the Fig. 7 is for a target type reverser without a kicker plate and is included for the comparison purposes. There will also be a secondary vortex at the exhaust of the engine as shown in zone 12, the strength of which is dependent on the thrust setting.

3.7 Flow behavior of the CMTTTR as seen on the vertical plane from the engine center line

This section discusses the flow characteristics of the CMTTTR in the vertical plane. Two streamline plots are constructed; Fig. 17a shows the flow behavior in a larger domain and Fig. 17b shows the reverser flow characteristics in the immediate vicinity of the engine.

For explanation purposes, the streamline plot in Fig. 17a is divided into four zones (i.e. zone 13, 14 15 and 16). Streamlines in Zone 13 show that at static conditions, the atmospheric air entering the engine is drawn from the downstream region. The actual downstream distance from where the streamlines will start is dependent on the engine thrust setting. Typically, the starting point is where the core thrust loses momentum: this means at high power the distance will be larger, but at low thrust settings this distance could be around 120 m (Fig. 17c). Streamlines in Zone 14 are mainly straight and represent the flow over the top of the nacelle, pylon and wing. As the streamlines approach the surfaces, they converge: this means that the flow over the top of the nacelle will accelerate as it approaches the engine inlet. The stagnation point appears to be near the trailing edge of the wing suction surface. The flow after the stagnation point will travel in the direction of engine inlet. The shape and behavior of the streamlines in zone 15 is highly dependent on the flow conditions in zone 14 and zone 16. The streamlines in zone 16 represent the behavior of

core flow. At the exit of the core nozzle, the streamlines are initially packed and uniform; however, as the core flow travels further away from the nozzle, the distance between the streamlines increases; the flow is losing momentum and dissipating its energy to the surroundings.

A vertical streamline plot, at a low thrust setting in which the FNPR≈1.20 (Fig. 17c), is also included in this study; the main objective is to show the comparison between the flow fields at high and low thrust settings. As previously stated, the shape of the external flow fields in zone, 13, 14, 15, and 16 is very much thrust dependent. At low thrust settings, two large contra-rotating vortices are observed downstream of the engine. The formation of these vortices is mainly because at low thrust settings the core flow will lose its momentum at a relatively shorter distance. However, when the engine thrust is increased, the front vortex will become stronger and stronger; the intensity of the second vortex (i.e. shorter vortex) which is due to the core exhaust flow will reduce, and will eventually disappear leaving either one large re-circulating vortex or no re-circulation zone. The importance of this discussion is to show that TR deployment and its effect on the downstream flow field is an important criterion that needs to be well understood for any TR design, as large disturbances in flow fields can affect the other approaching aircraft.

Zone 17 represents the flow at the engine front and upper half region of the nacelle. The vertical streamline plot shows that there is strong flow over the nacelle, which is due to the strong entrainment effect caused by the engine inlet flow. This flow then washes over the front of the nacelle upper surface and bends at almost 180 degrees to enter the engine. This excessive turning can result in a separation bubble at the leading edge of the nacelle.

The streamlines in zone 18 represent the reverser exhaust flow in the bottom half of the nacelle. The flow will initially impinge on the runway surface and will travel upstream towards the inlet. In order for this flow to enter the engine, it will turn at approximately 180 degrees around the bottom half of the nacelle. As this flow is coming from the engine core section, it will be at a higher temperature and pressure to that of zone 17: thus, at static conditions, there will be severe pressure and temperature distortion.

The aggressive turning of flows in zone 17 and 18 will create an outer boundary region (i.e. represented by the outermost streamlines). Outside this outer boundary region is zone 19, where the flow approaching from the top will meet the runway. It is noticed that this outer boundary flow will be present in both low and high thrust settings. Streamlines in zone 20 show the flow behavior over the top of the wing, pylon and nacelle; as the flow approaches these surfaces it will accelerate and will travel forward before being turned at high angles to enter the engine. Zone 21 represents the core exhaust flow; the flow is mostly straight; however, some disturbance is noticed due to reverser

Journal of Engineering for Gas Turbines and Power. Received August 17, 2017;
Accepted manuscript posted December 25, 2017. doi:10.1115/1.4038817

deployment: a small amount of core flow will travel in the direction of the reverse exhaust flow, after which it will travel along the runway as shown in (Fig. 17).

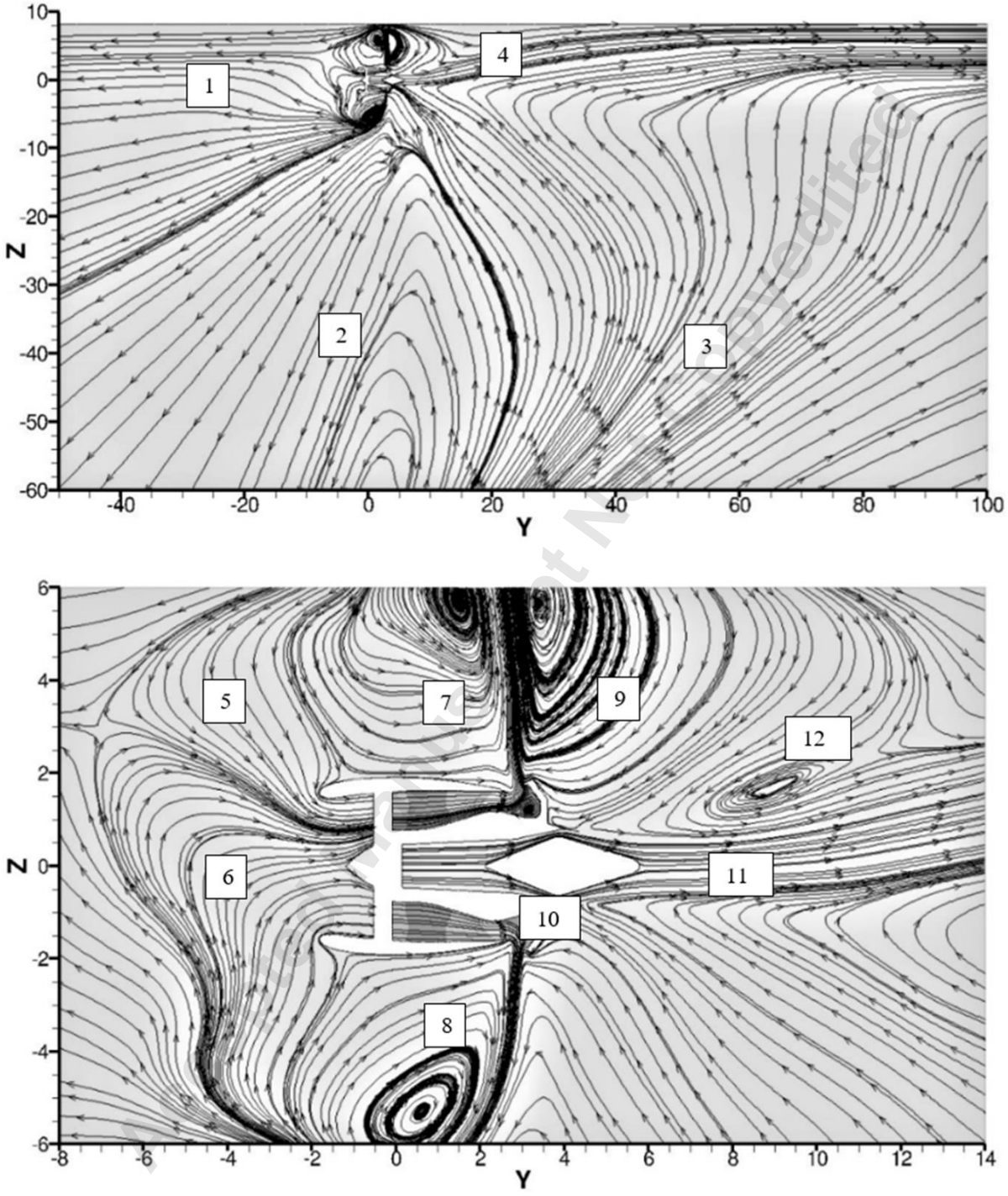

Fig. 16: (a) Streamlines plot in the horizontal plane from engine center line, FNPR=1.57, Mach=0.0. (b) shows the zoomed-in view of the streamline plot.

Journal of Engineering for Gas Turbines and Power. Received August 17, 2017;
Accepted manuscript posted December 25, 2017. doi:10.1115/1.4038817

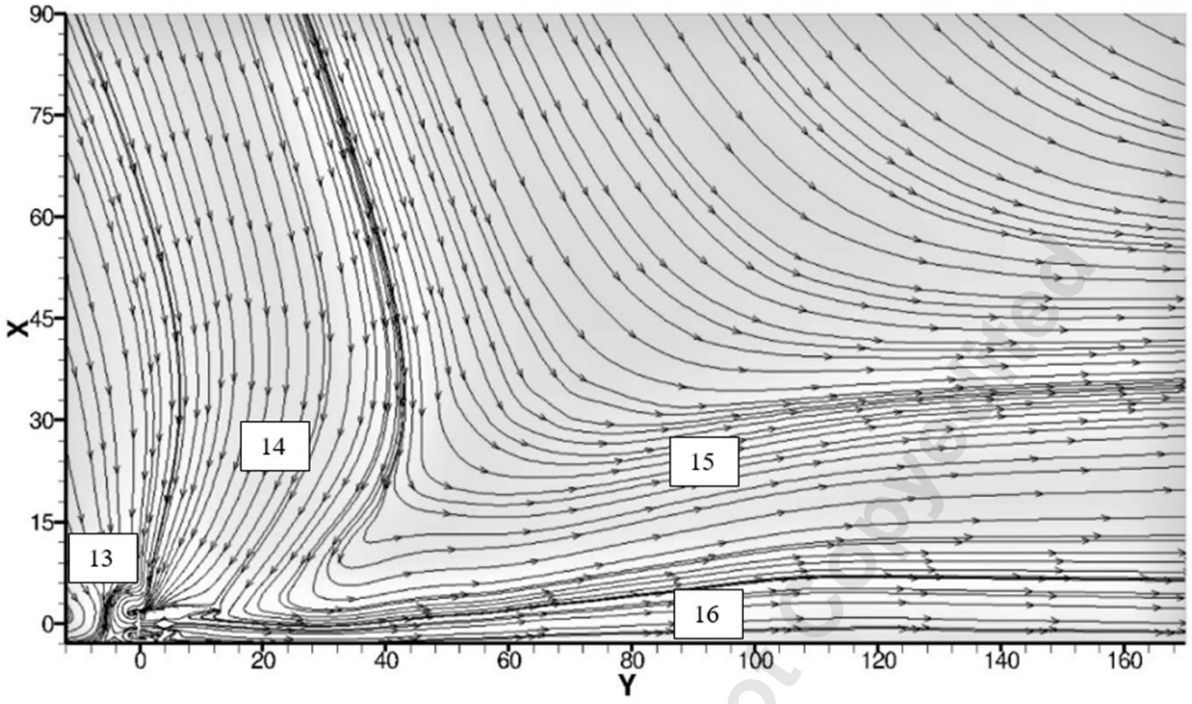

(a) Streamlines plot in the vertical plane from engine center line, FNPR=1.55, M=0.0.

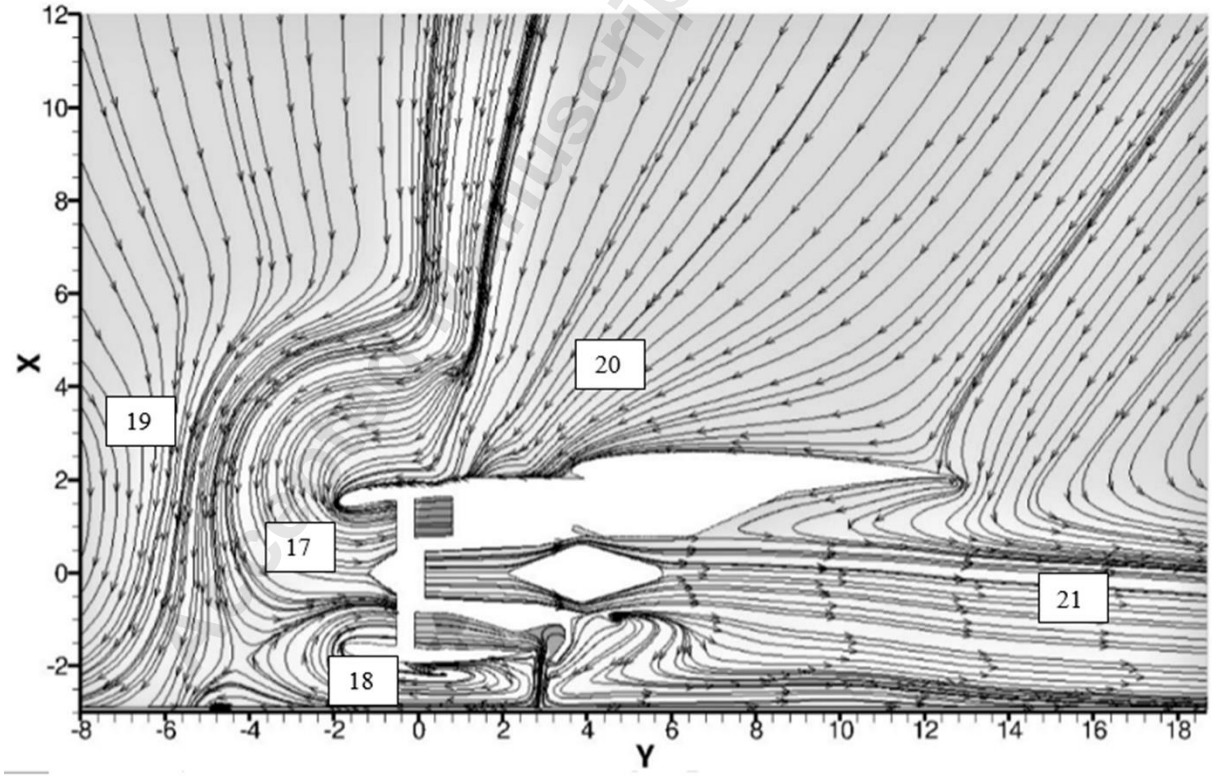

(b) Zoomed in view of the streamline plot.

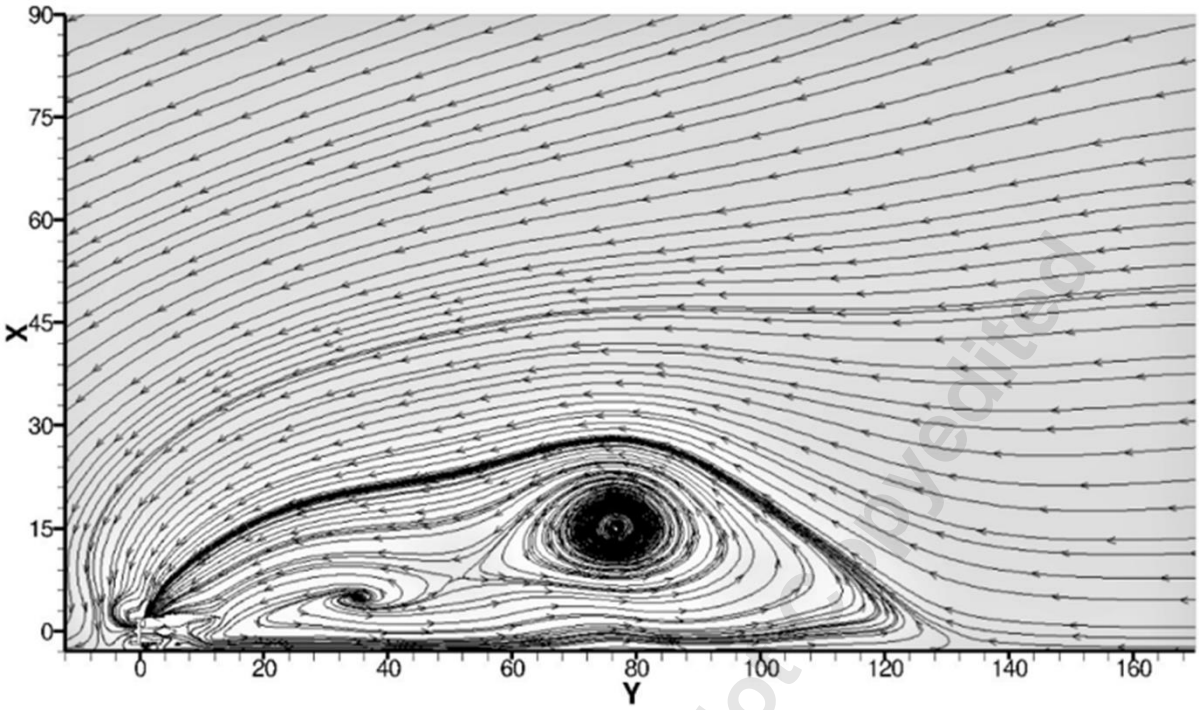

(c) Streamline plots in the vertical plane at FNPR=1.22, M=0.0.

Fig. 17: (a) Streamlines plot in the vertical plane from engine center line, FNPR=1.55, M=0.0. (b) Zoomed in view of the streamline plot. (c) Streamline plots in the vertical plane at FNPR=1.22, M=0.0.

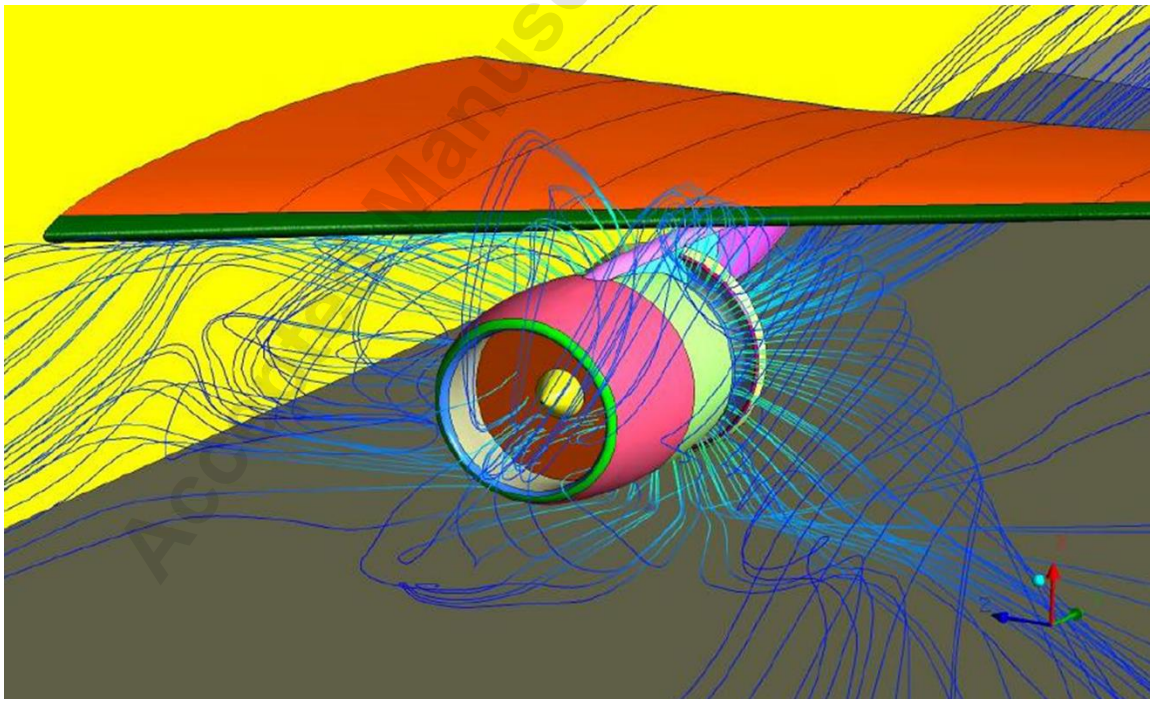

(18a) Frontal view

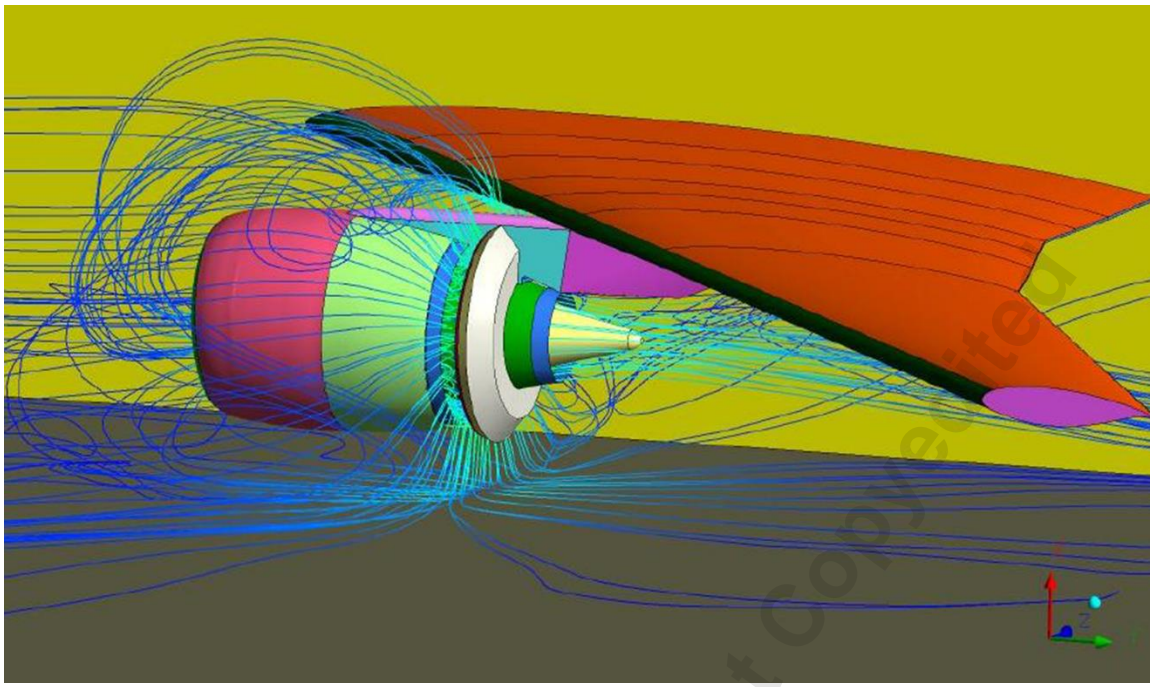

(18b) side view.

Fig. 18: Shows the typical flow behavior for the CMTTTR at static condition, M=0.0. (a) Frontal view, (b) side view.

4. Conclusion

An extensive assessment of a Core Mounted Target Type Thrust Reverser (CMTTTR) design in deployed configuration at static aircraft conditions is presented in this paper. Full-scale 3D CFD analyses are performed at SLS ISA conditions and the results are validated with the experimental data: the acquired results exhibit good agreement with the experiments. The results from the CFD analyses are used to assess the performance of the CMTTTR both with and without the kicker plate: it is observed that the CMTTTR design failed to produce any effective reverse thrust. Further, it is noted that the CMTTTR design failed to meet the mandatory mass flow compatibility criteria by approximately 40%. From the CFD analyses it is observed that majority of the flow will travel in the radial direction, with only a small amount of flow travelling axially: this resulted in CMTTTR producing a significant amount of radial force instead of axial, which is mainly attributed to the CMTTTR design.

Overall reverser effectiveness for the CMTTTR design is assessed by CFD and found to be in good agreement with the test results; however, the CFD analyses showed that no reverse thrust is produced and the axial force generated is, in fact, acting in the direction of core thrust (i.e. producing forward force instead of reverse force), whereas the

results from the tests showed that a small amount of reverse force is generated. Both these forces are very close; however, one is positive and the other is negative: this may be attributed to the difference in the experimental and computational setup as well as the difference in measuring techniques, or perhaps may be due to the installation of a wing.

In this paper, Pressure Thrust is also estimated. The Pressure Thrust is defined as the axial force produced due to the difference in pressure across the reverser target surfaces. A new formula for the estimation of the overall reverser effectiveness is proposed, which considers the Pressure Thrust force. From the information, available in the public domain, this may be the first paper highlighting the importance of estimating Pressure Thrust and including it in the formula of overall reverser effectiveness. It is also observed from the CFD analyses that the installation of kicker plate not only helps in enhancing the reverser axial component but also helps to improve the Pressure Thrust value, which in turn increases the overall reverse thrust. Finally, reverser flow characteristics corresponding to the reverser deployed configuration are thoroughly examined using the 2D horizontal and vertical streamline plots.

5. Acknowledgments

This work was supported by Cranfield University, Centre for Propulsion Engineering. The main author would like to thank and acknowledge Anthony Jackson for his guidance and significant expertise in engine design, performance and aerodynamics. Special thanks to Vishal Sethi for his guidance and supervision of this complex project. Thanks to Bidur Khanal for his knowledge and expertise in CFD and post processing. In the end, special thanks to Fakhre Ali, for his valuable suggestions, advice and expertise in turbomachinery design and performance.

References

[1] Scott C. A., “Static Performance of Six Innovative Thrust Reverser Concepts for Subsonic Transport Applications: Summary of the NASA Langley Innovative Thrust Reverser Test Program”, TM-2000-210300, NASA - Langley Research Centre, Hampton, Virginia.

[2] Khanal. B., Mahmood. T., Ali. F., “CFD Investigation of a Core-Mounted Target-Type-Thrust-Reverser, Part 1: Reverser Stowed Configuration”.

[3] Chuck. C., "Computational Procedure for Complex Three-Dimensional Geometries Including Thrust Reverser Effluxes and APUs"., AIAA-2001-3747., 37th AIAA Joint Propulsion Conference, 8th – 11th July, 2001, Salt Lake City, Utah.

[4] Andrade. F. O., Ferreira. S. B., Silva. L. F. F., Jesus. AA. B., Oliveira. G. L., "Study of the Influence of Aircraft Geometry on the Computed Flowfield During Thrust Reversers Operation"., 24th AIAA Applied Aerodynamic Conference, 5th – 8th June, 2006, San Francisco, California.

[5] Trapp. L. G., and Oliveira. G. L., "Aircraft Thrust Reverser Cascade Configuration Evaluation Through CFD"., 41st AIAA Aerospace Meeting and Exhibition, 6th - 9th January, 2003, Reno, Nevada.

[6] Turpin. G., Vuillot. F., Croisy. C., Bernier. D., Mabboux. G., "Numerical Simulation of Thrust Reverser for Rear Mounted Engine", Published by Onera and Safran Group.

[7] FLUENT 6.3 User's Guide. Fluent Inc, 2006.

[8] GasTurb 10, Performance Software

CFD investigation of a core-mounted-target-type thrust reverser, Part 2: reverser deployed configuration

Mahmood, Tashfeen

2017-12-25

Tashfeen Mahmood, Anthony J B Jackson, Vishal Sethi et al. CFD investigation of a core-mounted-target-type thrust reverser, Part 2: reverser deployed configuration. Journal of Engineering for Gas Turbines and Power, 2018, Volume 140, Issue 9, Article number 091205, Paper number GTP-17-1465

http://dx.doi.org/10.1115/1.4038817